


**DETECTION AND CLASSIFICATION OF BREAST LESIONS IN BIOMEDICAL IMAGES  
IN AN EXPLAINABLE WAY**

**DETECÇÃO E CLASSIFICAÇÃO DE LESÕES MAMÁRIAS EM IMAGENS BIOMÉDICAS  
DE FORMA EXPLICÁVEL**

**DETECCIÓN Y CLASIFICACIÓN DE LESIONES MAMARIAS EN IMÁGENES  
BIOMÉDICAS DE FORMA EXPLICABLE**

 <https://doi.org/10.56238/arev7n9-289>

**Submission date:** 08/26/2025

**Publication date:** 09/26/2025

**Gabriel Luiz Limeira Barreto<sup>1</sup>, Sidney Marlon Lopes de Lima<sup>2</sup>**

---

**ABSTRACT**

**Purpose:** Breast cancer is a major public health issue and the leading cause of cancer death among adult women in Brazil. Late diagnosis contributes to high mortality rates and invasive surgeries. Limited access to imaging tests results in diagnoses at advanced stages, underscoring the need for early detection to improve cure rates and avoid aggressive procedures. The objective of this study is to enhance breast cancer diagnosis, particularly in countries with prevalent late diagnoses, by applying advanced artificial intelligence and extreme learning techniques to thermographic images.

**Methods:** The study utilizes advanced artificial intelligence (AI) and extreme learning techniques to analyze thermographic images. The goal is to develop a computer system that not only accurately diagnoses breast cancer but also provides explanations for its decisions in a way that healthcare professionals can understand.

**Results:** The proposed AI approach demonstrated efficiency in detecting and classifying breast lesions in thermographic images. The system achieved an accuracy of 89.70% in distinguishing malignant lesions from other diagnoses in its best-case scenario.

**Conclusion:** The developed system represents a significant advancement in breast cancer diagnosis, particularly in regions where late-stage diagnoses are common. It holds potential to improve diagnostic accuracy, contribute to better patient outcomes, and enhance recovery prospects for breast cancer patients.

**Keywords:** Breast Lesions. Breast Cancer. Biomedical Imaging. Machine Learning.

**RESUMO**

**Objetivo:** O câncer de mama é um importante problema de saúde pública e a principal causa de morte por câncer entre mulheres adultas no Brasil. O diagnóstico tardio contribui para altas taxas de mortalidade e cirurgias invasivas. O acesso limitado a exames de imagem

---

<sup>1</sup> Department of Computer Engineering. Universidade de Pernambuco (UPE). Recife, Brazil.  
E-mail: gllb@ecom.poli.br Orcid: 0009-0000-9120-3994 Lattes: <https://lattes.cnpq.br/3481187860569549>

<sup>2</sup> Department of Electronic Engineering. Universidade Federal de Pernambuco (UFPE). Recife, Brazil.  
E-mail: sidney.lima@ufpe.br Orcid: 0000-0002-4350-9689 Lattes: <http://lattes.cnpq.br/0323190806293435>

resulta em diagnósticos em estágios avançados, reforçando a necessidade de detecção precoce para aumentar as taxas de cura e evitar procedimentos agressivos. O objetivo deste estudo é aprimorar o diagnóstico do câncer de mama, particularmente em países com diagnóstico tardio prevalente, aplicando inteligência artificial avançada e técnicas de aprendizado extremo a imagens termográficas.

**Métodos:** O estudo utiliza inteligência artificial avançada (IA) e técnicas de aprendizado extremo para analisar imagens termográficas. O objetivo é desenvolver um sistema computacional que não apenas diagnostique o câncer de mama com precisão, mas também forneça explicações para suas decisões de forma compreensível para os profissionais de saúde.

**Resultados:** A abordagem de IA proposta demonstrou eficiência na detecção e classificação de lesões mamárias em imagens termográficas. O sistema alcançou uma acurácia de 89,70% na distinção de lesões malignas de outros diagnósticos em seu melhor cenário.

**Conclusão:** O sistema desenvolvido representa um avanço significativo no diagnóstico do câncer de mama, particularmente em regiões onde diagnósticos em estágio avançado são comuns. Ele tem potencial para melhorar a precisão diagnóstica, contribuir para melhores resultados para os pacientes e aumentar as perspectivas de recuperação de pacientes com câncer de mama.

**Palavras-chave:** Lesões Mamárias. Câncer de Mama. Imagem Biomédica. Aprendizado de Máquina.

## RESUMEN

**Objetivo:** El cáncer de mama es un importante problema de salud pública y la principal causa de muerte por cáncer en mujeres adultas en Brasil. El diagnóstico tardío contribuye a las altas tasas de mortalidad y a las cirugías invasivas. El acceso limitado a la imagenología resulta en diagnósticos en estadios avanzados, lo que refuerza la necesidad de la detección temprana para aumentar las tasas de curación y evitar procedimientos agresivos. El objetivo de este estudio es mejorar el diagnóstico del cáncer de mama, especialmente en países con prevalencia de diagnóstico tardío, mediante la aplicación de inteligencia artificial avanzada y técnicas de aprendizaje extremo a imágenes termográficas.

**Métodos:** El estudio utiliza inteligencia artificial (IA) avanzada y técnicas de aprendizaje extremo para analizar imágenes termográficas. El objetivo es desarrollar un sistema computacional que no solo diagnostique con precisión el cáncer de mama, sino que también proporcione explicaciones de sus decisiones de forma comprensible para los profesionales sanitarios.

**Resultados:** El enfoque de IA propuesto demostró eficiencia en la detección y clasificación de lesiones mamarias en imágenes termográficas. El sistema alcanzó una precisión del 89,70 % al distinguir lesiones malignas de otros diagnósticos en el mejor de los casos. **Conclusión:** El sistema desarrollado representa un avance significativo en el diagnóstico del cáncer de mama, especialmente en regiones donde los diagnósticos en etapas avanzadas son frecuentes. Tiene el potencial de mejorar la precisión diagnóstica, contribuir a mejores resultados para las pacientes y aumentar las perspectivas de recuperación de las pacientes con cáncer de mama.

**Palabras clave:** Lesiones Mamarias. Câncer de Mama. Imágenes Biomédicas. Aprendizaje Automático.

## 1 INTRODUCTION

### 1.1 BREAST CANCER

Breast cancer is a significant public health concern and is the leading cause of cancer-related deaths among adult women in Brazil [1]. This disease manifests without distinction between countries with varying levels of social and economic development. However, there has been an increase in breast cancer incidence rates in economically developed countries such as the United States, Canada, and the United Kingdom since the 21st century, associated with rising obesity and sedentary lifestyles in these nations [2].

Despite the high incidence of breast cancer in developed countries, mortality rates are relatively low compared to developing nations. Although breast cancer incidence in Europe in 2022 was higher than in Africa (563,431 versus 198,831 new cases per year), the breast cancer mortality rate was comparable (14.7% versus 19.2%) [3]. This disparity can be attributed to the limited access to breast imaging examinations in Africa, leading to cancer diagnoses at more advanced stages, which profoundly impacts breast cancer survival rates on the continent. This situation not only results in higher mortality but also leads to more radical surgical interventions, such as mastectomy.

In developing and emerging nations, mortality rates can be attributed to the late diagnosis of cancer [2]. It is significant to note that the initial manifestation of symptoms can take up to a decade to become detectable through palpation. It is estimated that the period between the onset of the lesion and its growth to a palpable size of approximately 1 cm is around 10 years [4]. Approximately 12.7% of cancer deaths among women worldwide in 2022 were due to breast cancer [3]. The availability of specialized breast imaging procedures, combined with accurate interpretation, plays a crucial role in the early detection of the disease, thereby increasing the chances of patient recovery.

Surgeries such as mastectomy are being avoided because the loss of a breast generally causes serious damage to a person's self-esteem, potentially leading to chronic depression. However methods for restoring the breast's shape, such as reconstruction surgery using the TRAM technique and breast prostheses, are now available.

Despite breast reconstruction, many patients experience depressive states. One reason is that the sensitivity of a reconstructed breast is not the same as that of the original breast tissue. Many women, for instance, report sensations of numbness in the new breast [4]. It is emphasized that patients undergoing breast-conserving therapy can live, on average,

as long as those undergoing mastectomy surgery [4]. Early cancer detection through imaging exams plays a crucial role in the decision for breast-conserving therapy [2].

## 1.2 DIGITAL PROCESSING OF BIOMEDICAL IMAGES

The application of technologies in medical imaging has proven to be a crucial tool for supporting surgical procedures and related simulations, planning radiotherapy treatments, and monitoring the progression of pathological conditions. Detailed analysis of anatomical forms and structures enables surgeons to devise highly efficient approaches. In the context of radiotherapy, medical images allow for precise assessment of the location and doses of radiation delivered to the tumor site, thereby minimizing the impact on healthy tissues.

Despite the exceptional resolution of internal human anatomy provided by imaging devices, the analysis of pathologies through images remains a complex task, primarily due to the extensive variation in clinical cases. Many instances encountered in clinical practice do not precisely align with traditional images and descriptions [5]. Additionally, there is a significant challenge in interpreting lesion configurations in images affected by interferences, such as those arising from ultrasound equipment or mammography. Various studies indicate that more than 70% of suspected breast cancer cases that proceed to biopsy are benign lesions [6], [7], [8].

Mammography continues to be regarded as the most effective technology for breast cancer diagnosis due to its widespread use and the interpretability of the images obtained. In this examination, compression between two specially designed plastic plates, which provide uniform and controlled compression, ensures a sharp and precise image. The primary objective is to detect early malignant lesions in the breast, and it is indicated for evaluating suspicious mammary findings at any age, in both men and women [1].

According to the guidelines of the Brazilian Ministry of Health, it is recommended that women over 40 years of age undergo this examination annually, while those with risk factors should do so every 6 months starting at age 35. For women between 50 and 69 years old, mammography is recommended every two years [2].

Considering the classification by the American College of Radiology (ACR), it is possible to observe a scale that divides lesions into five groups: regular, lobular, microlobular, irregular, and spiculated, as illustrated in Figure 1 [9]. A lesion classified as regular often encompasses benign findings, such as simple cysts, fat tissue nodules, or benign calcifications. The edges of these lesions tend to be smooth and well-defined, with few

noticeable irregularities. They typically exhibit a uniform and symmetrical appearance on mammographic images [9].

Lesions classified as lobular are generally characterized by curvilinear and undulating contours. These lesions may indicate conditions such as fibroadenomas, which are common benign findings in the breast's glandular tissue, or ductal hyperplasia, a benign proliferation of cells in the mammary ducts. The texture of these lesions may appear denser and more compact compared to regular lesions [9].

Microlobulated lesions present small protrusions or bumps along the edge and may suggest the presence of benign microcalcifications, such as those associated with fibrosis or adenosis, or adenomatous lesions, which are benign masses formed by glandular tissue. These lesions may also exhibit granular or grainy areas on mammographic images [9].

Spiculated lesions display projections or radiating lines at the margins, which may be an indicator of malignant tumors, such as invasive breast carcinomas. The presence of irregular and sharp spicules around the lesion increases the suspicion of malignancy. These spicules may appear irregular and uneven, with serrated or branching edges. The group of irregular lesions is highly diverse and encompasses a wide range of findings, from congenital anomalies to advanced malignant tumors. Irregular lesions may exhibit highly variable shapes and edges, making their characterization more challenging. They may appear distorted, asymmetrical, or lack a defined pattern on mammographic images [9].

The ACR BI-RADS® also establishes standards regarding lesion density. Theoretically, malignant lesions tend to present a density higher than that of the breast, while lesions with density lower than that of the breast are generally benign. For example, lesions with fat density are benign in the vast majority of cases [9].

In the digital technology era, numerous "second-opinion" tools have emerged to enhance and complement the diagnostic process conducted by specialists. These tools, often based on advanced algorithms and artificial intelligence, provide an additional layer of data analysis and interpretation, offering valuable assistance to healthcare professionals in making diagnostic decisions. By providing additional, comparative, or complementary insights to the results obtained by specialists, these digital tools not only expand the range of available resources but also can increase the accuracy and confidence of diagnoses, leading to better prognoses and treatments for patients.

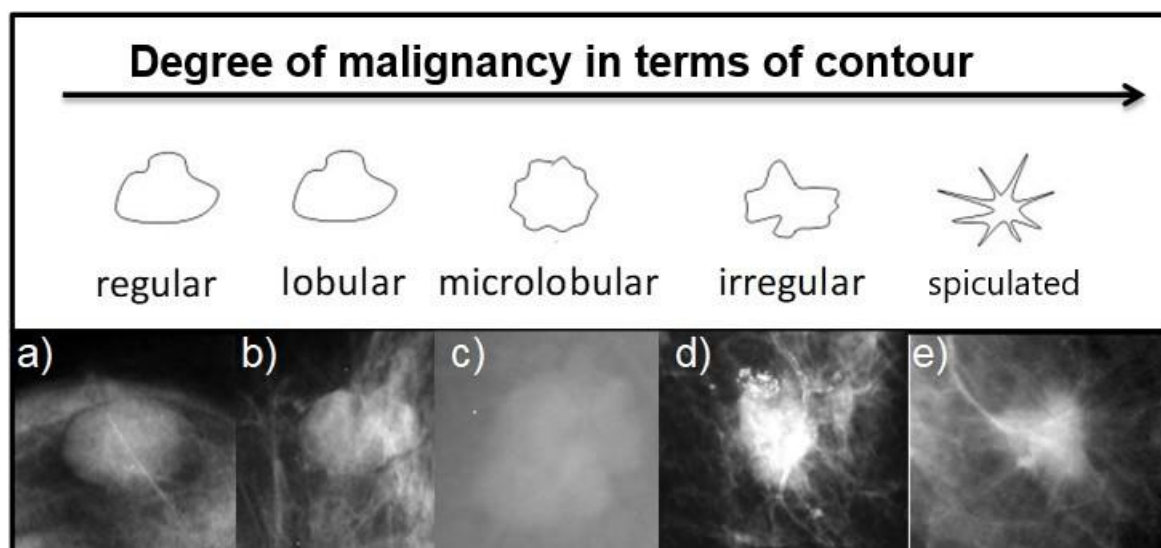
The identification and classification of breast lesions through imaging exams can be significantly influenced by the feature extraction stage. Among the commonly used

approaches, segmentation plays a prominent role. This technique aims to separate the lesion from other components present in the image, enabling a more detailed and accurate analysis. As a result, statistical and geometric metrics are derived from the area occupied by the cellular anomaly and compared with its surrounding region. To achieve this goal, segmentation techniques, adopted in advanced approaches, typically operate in the area corresponding to the image plane itself, where the methods are based on the direct manipulation of pixels.

"Second-opinion" tools result in a better characterization of breast lesions and, consequently, a more accurate evaluation of mammography results. Figure 2 shows manual segmentations performed by radiologists from the DDSM Database for Screening Mammography} database [10], which is widely used in state-of-the-art research. In addition to the data provided by the DDSM, state-of-the-art research often employs private radiologists to segment the original mammogram and/or improve the performance of proposed image processing techniques during their execution. It is observed that the freehand traces, presented in Figure 2b and Figure 2d, made by specialists, generated patterns that did not correspond to the gradients of the images under study.

**Figure 1**

*Classification of the lesion in terms of contour according to BI-RADS*



Source: de Lima et al. (2014) [11].

Specialists also delineated spiculations that were not properly outlined in the original images, as illustrated in Figure 2a and Figure 2c. A lesion with spiculated characteristics exhibits radiating lines that originate from its interior and extend toward its edges, often indicating malignant features [9]. It is evident, therefore, that these manual segmentations not only isolated the lesions but also implicitly performed the subsequent step of classifying benign and malignant nodules.

Based on these approaches, it becomes clear that the most challenging part of the interpretation and execution process is attributed to the specialists who perform the detection and classification of the lesion. Meanwhile, computational techniques benefit from the meticulous work of the specialist both during the application phase and the testing phase.

In addition to segmentation, current advancements in the field require specialists to make adjustments to the performance of the proposed image processing techniques. This type of human involvement can be quite time-consuming. The complexity arises because mammographic images typically display varying degrees of intensity in grayscale. Thus, a single threshold is rarely sufficient to accurately delineate the entire lesion boundary. Manually adding or removing parts of these segments allows for interference in the feature extraction step. Consequently, when deriving statistical and geometric measures between the manually identified area that shows tissue distortion and its adjacent region, the result can differ significantly from the actual image content, impacting lesion classification. The current state-of-the-art does not provide details on how specialists adjust the performance of image processing techniques.

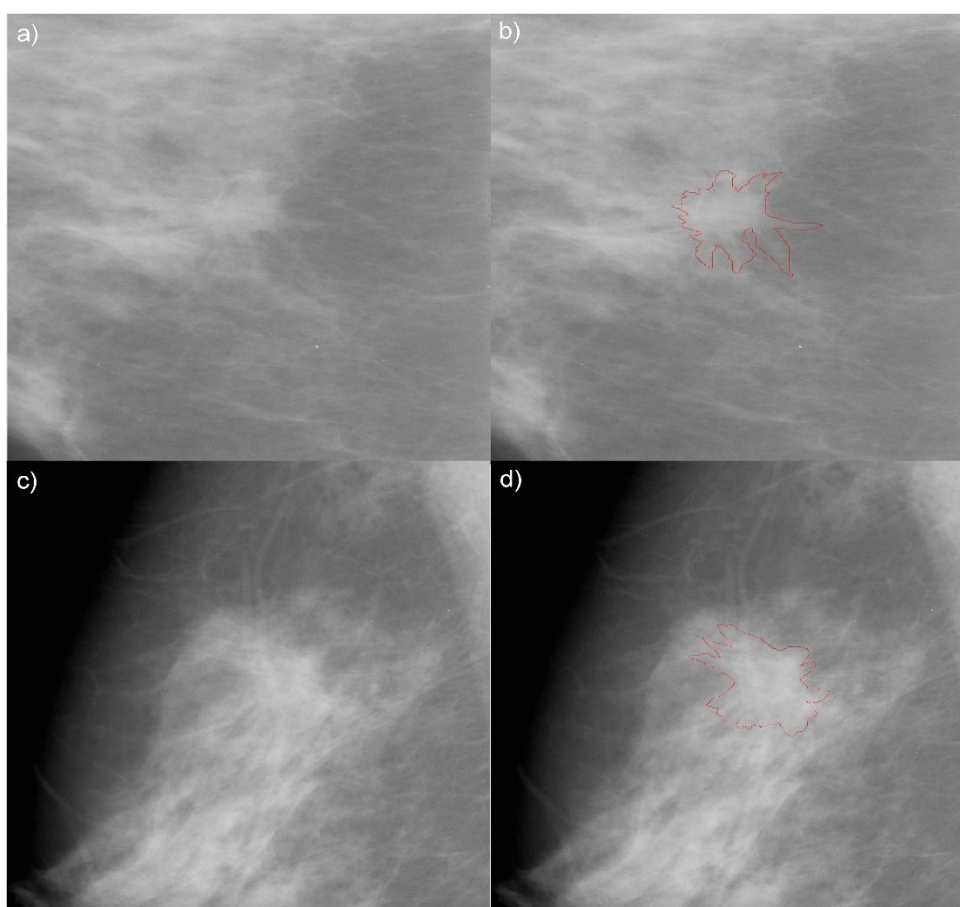
In addition to segmentation, current advancements in the field require specialists to make adjustments to the performance of the proposed image processing techniques. This type of human involvement can be quite time-consuming. The complexity arises because mammographic images typically display varying degrees of intensity in grayscale. Thus, a single threshold is rarely sufficient to accurately delineate the entire lesion boundary. Manually adding or removing parts of these segments allows for interference in the feature extraction step. Consequently, when deriving statistical and geometric measures between the manually identified area that shows tissue distortion and its adjacent region, the result can differ significantly from the actual image content, impacting lesion classification. The current state-of-the-art does not provide details on how specialists adjust the performance of image processing techniques.

It is inferred that an image editing software and/or custom software may be essential for establishing local thresholds or adjusting processing parameters for each micro-region of the lesion. Furthermore, healthcare professionals may face challenges when handling image editing software, especially during busy shifts when radiologists may struggle to perform time-consuming tasks. However, more advanced computational approaches are being utilized to broaden the scope of lesion detection applications in mammography.

According to the latest trends, deep learning methodologies demonstrate superior performance compared to shallow intelligent techniques in terms of breast lesion classification and detection rates. Deep and shallow learning refer to techniques with high and low computational complexity, respectively. Deep learning can directly manipulate the original image and is not limited to working solely with the results of manual segmentation, as is common in current practice during mammographic examinations.

## Figure 2

*Manual segmentations by radiologists*



Source: Adapted from the DDSM database (Digital Database for Screening Mammography - Digital Database of Digitized Mammograms) Heath and Bowyer. (2000) [10].

### 1.3 JUSTIFICATION

Despite representing the state-of-the-art in biomedical engineering, Deep Learning presents several limitations. Deep learning techniques require computers with high processing and storage capacities, and training can take months or even years, even on a powerful computer (server).

The limitations of deep neural models can be addressed by artificial intelligence techniques based on extreme learning. Extreme learning neural networks represent a class of computational intelligence models that, through their learning processes, enable the construction of nonlinear mappings of data. These techniques have very low computational complexity yet can achieve excellent accuracies [12], [13], [14], [15], [16]. As an advantage, it is feasible to explain the functioning of extreme learning to a human due to the low amount of calculations involved.

This research aims to employ extreme learning in the identification and classification of breast lesions in thermographic images. The use of thermography in breast cancer detection has been applied for more than ten years [17], [18], [19], [20], [21], [22]. This method seeks to employ techniques with minimal side effects for both the patient and the specialist professional. Because breast thermography does not involve ionizing radiation, it can be considered a promising alternative for functional and metabolic evaluations of the breast, complementing conventional imaging techniques. Unlike mammography, thermography is suitable for women of all ages, including pregnant or breastfeeding women, those with breast implants, high breast density, fibrocysts, or those undergoing hormone replacement therapy. It can be performed on both premenopausal and postmenopausal women [17]. The exam involves capturing an image that reflects the temperature distribution on the skin's surface, specifically the superficial temperature of the breast.

However, it is not enough for the computational technique to operate correctly on thermographic images. Biomedical engineering mechanisms must be capable of explaining their own functioning. It is necessary for the knowledgeable professional to be fully convinced that the "second-opinion" tool is useful. Through self-explainable computing, the artificial intelligence tool becomes capable of explaining its diagnoses in a creative and intelligent manner.

Based on Alan Turing's postulates, a machine capable of explaining itself to a human is the closest approximation to a machine capable of thinking [23]. The limitations of anatomical disease detection mechanisms are evident when compared to Alan Turing's

postulates. Diagnoses provided by computational tools conventionally occur through labels without further clarification. The deep learning computational tool simply identifies whether the patient has cancer but does not offer any support to the specialist professional to justify their decision.

When considering thermography images, the goal is to establish descriptions and patterns similar to the work done by the American College of Radiology in BI-RADS. The motivation stems from the fact that the lesions found in thermography currently do not present a self-descriptive technical standard. Self-explainable artificial intelligence becomes a good alternative because, during its training phase, it can analyze thousands of files and extract characteristics from them. After learning, self-explainable artificial intelligence would be able to establish patterns regarding the shape, density, and surrounding area of the lesion. In this way, the technique would gain the means to support its decision to a human.

The tool would provide resources so that the qualified professional could defend themselves before the professional council, for example.

#### 1.4 GENERAL OBJECTIVE

To propose an intelligent method for the detection and classification of breast lesions in biomedical images using extreme neural networks in thermography. The proposed method will be designed with the intrinsic ability to explain its own functioning in a manner understandable to humans. This will facilitate the persuasion of specialized professionals, demonstrating that the tool can provide an accurate and valuable "second opinion." The intelligent biomedical technique developed will have the capability to present its diagnoses creatively and intelligibly. As our specific objectives:

- Study techniques and algorithms for digital processing in biomedical images.
- Adapt the selected computational techniques to address problems encountered in clinical practice, which differ from classical images and descriptions.
- Define the experimental environment.
- Analyze the results.
- Validate the proposed intelligent system model within the academic community.

#### 1.5 STATE OF THE ART

Table 1 presents a list of state-of-the-art intelligent techniques applied to thermograms and mammograms. These include machine learning algorithms, neural networks, and feature

selection methods. Intelligent techniques have shown promising results in the early detection and classification of breast anomalies.

**Table 1**

*Summary of Key State-of-the-Art Intelligent Techniques*

Authors	Neural Network Type	Objective	Accuracy
Authorial AI (Self-explainable)	Shallow network	Feature extraction + Pattern recognition	89.70%
PEREIRA et al. (2021)[17]	Shallow network	Feature pruning + Pattern recognition	84.93%
Mariana (2021)[24]	Deep + Shallow network	Feature pruning + Pattern recognition	87.25%
Santana (2022)[25]	Deep + Shallow network	Pattern recognition	≈84%
Santana2 (2022) [26]	Deep + Shallow network	Pattern recognition	≈85%

Source: The author (2024).

Pereira et al.(2021)[17] proposed an attribute selection method based on the dialectical optimization technique applied to breast thermography. The aim was to simplify the classifiers and enhance their generalization capability to support the diagnosis of breast lesions. The proposed attribute selection technique enabled the simplification of classifier architectures by reducing the dimensionality of feature vectors by approximately 50%, with minimal impact on classification accuracy only about a 3.72% reduction. The methodology by PEREIRA et al. (2021) is a promising technique for feature reduction, achieving significant accuracy values using only 84 out of the original 168 features extracted. This highlights the importance of this step for employing breast thermography as an auxiliary technique in breast cancer diagnosis. PEREIRA et al. (2021) achieved an accuracy of 84.93% after reducing the number of input features in the application [17].

Macedo et al.(2021) [24] implemented a methodology for the identification and classification of lesions using real patient images from Brazilian women, combining characteristic models, feature selection, and classification using machine learning algorithms. The study emphasizes the relevance of breast thermography, which can detect metabolic changes associated with lesions. The proposed method extracts shape and texture features using Zernike and Haralick moments, reducing the amount of data by 50%. Feature selection is performed using swarm intelligence-based optimization algorithms, contributing to computational efficiency without compromising accuracy. Eleven machine learning algorithms, including convolutional neural networks and support vector machines, were

evaluated for image categorization. The results show that the proposed approach reduces computational time while maintaining high classification rates. The study highlights the role of feature selection in diagnostic accuracy, especially concerning shape-related aspects. It contributes to the development of less painful and more efficient alternatives for breast cancer diagnosis, particularly in regions with limited resources and access to specialists. The highest accuracy achieved was 87.25% [24].

Santana et al.(2022a) [25] proposed a deep hybrid architecture to support the diagnosis of breast thermographic images, based on five-layer Deep Wavelet Neural Networks for extracting features from regions of interest in mammograms and support vector machines with linear kernels for final classification. Classical classifiers such as Bayesian classifiers, single-layer perceptrons, decision trees, random forests, and support vector machines were tested. By using a deep neural network with predefined weights from a Wavelet Transform filter bank, it was possible to extract features and reformulate the problem in a way that allowed for resolution with relatively simple decision boundaries, such as those generated by support vector machines with linear kernels. This demonstrates that such new deep networks may play an important role in building complete solutions to enhance the potential of breast thermography and support clinical diagnosis. The findings demonstrated the feasibility of identifying and classifying lesions with accuracy above 84% using transfer learning between Deep Wavelet networks and machine learning via random forests [25].

Santana et al. (2022b) [26] introduced innovative approaches using Deep Wavelet Neural Networks, which are convolutional and may use predefined filter banks as neurons. The study focused on breast thermography, a non-invasive technique, highlighting the importance of feature selection to improve diagnostic effectiveness. The results demonstrated the feasibility of lesion detection and classification. A second approach adopted digital mammography, proposing a deep hybrid architecture using six-layer Deep Wavelet Neural Networks. The study emphasizes the potential of deep neural networks that incorporate predefined filters, providing robust solutions to support breast cancer diagnosis. These promising approaches demonstrate the relevance of machine learning methods in improving mammographic image analysis, significantly contributing to early detection and effective breast cancer treatment. Santana et al. (2022b) [26] achieved an accuracy close to 85% using transfer learning between Deep Wavelet networks and machine learning via random forests.

## 2 METHODS

### 2.1 PRELIMINARY STUDIES: FEATURE EXTRACTION IN BIOMEDICAL IMAGES

The extraction of features from biomedical images presents significant challenges. Finding an appropriate feature extractor for one biomedical application does not guarantee its success in another. The variability of human anatomy and metabolism is extensive, and therefore, computational techniques may encounter operational problems when applied to biomedical images. Given these considerations, Zernike moments are a feature extraction technique capable of yielding promising results across a variety of biomedical scenarios, such as mammograms and thermograms [11], [12], [13], [14], [15], [16], [27].

### 2.2 ZERNIKE MOMENTS

Zernike moments are a series of mathematical coefficients that describe the shape of a two-dimensional surface, such as a lens, a thin film, or a circular aperture. These moments are often used in optics, computer vision, and other related fields to characterize the aberration and image quality of optical systems. They are named after the Dutch mathematician Frits Zernike, who developed this technique in 1934 and was awarded the Nobel Prize in Physics in 1953 for his work [28].

Zernike moments are calculated based on the polar coordinates of a surface around a central reference point. Each Zernike moment corresponds to a specific Zernike polynomial and represents a particular feature of the surface's shape. They can be used to quantify irregularities or deviations of a surface compared to an ideal shape, such as a perfect spherical surface [28].

The general form of the Zernike polynomial is:

$$Z_{n,m}(r,\theta) = R_{n,m}(r) \cdot e^{im\theta} \quad (1)$$

Where:

$n$  is a nonnegative integer that controls the number of radial lobes in the polynomial.

$m$  is an integer that determines the number of times the function wraps around the center.

$r$  is the radial distance from the polar coordinate to the center.

$\theta$  is the polar angle.

The Radial Zernike polynomials,  $R_m(r)$ , are derived through a recursive relation based on Legendre polynomials. They can be expressed as:

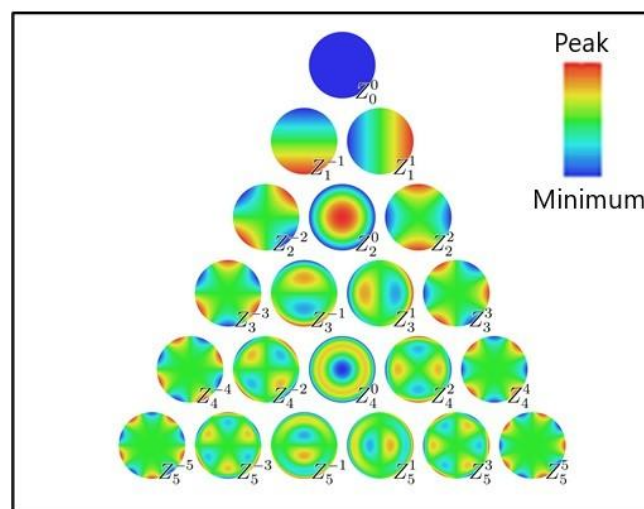
$$R_n^m(r) = \sum_{k=0}^{(n-m)/2} \frac{(-1)^k \cdot (n-k)!}{k! \cdot ((n+m)/2-k)! \cdot ((n-m)/2-k)!} \cdot r^{n-2k} \quad (2)$$

Some situations where Zernike moments can be utilized include:

- Characterization of optical aberrations: Zernike moments are used to quantify and describe distortions in optical systems, providing a deeper understanding of how imperfections affect the quality of the formed image.
- Adaptive astronomy: Zernike moments are employed in real time correction of atmospheric distortions in astronomical observations, thereby enhancing image clarity.
- Microscopic image analysis: They are utilized in the analysis of microscopic images, enabling the detection and characterization of optical distortions in microscopic systems.
- Evaluation of visual aberrations in the human eye: Zernike moments are used to assess visual distortions in the human eye, aiding in the prescription of customized corrective lenses.

**Figure 3**

*Magnitude of the Zernike moments' basis functions in disk units*



Source: Tahmasbi et al. (2011)[29].

Zernike moments play a crucial role in modern optics, enabling quantitative analysis of optical distortions and providing a solid mathematical foundation for correcting these

distortions. Their wide range of applications across various fields of optics makes them an essential tool for capturing images with optimal quality and accuracy.

Zernike moments have been extensively used to extract shape characteristics of breast lesions [12], [13], [14]. Shallow neural networks rely on feature extractors from raw data. Due to their low computational complexity, shallow networks lack mechanisms to convert raw data into a statistical learning repository. When employing shallow neural networks, the responsibility for detecting and categorizing breast lesions using mammograms is strongly influenced by the feature extraction phase [15].

Zernike moments can detail the evaluated lesion according to the criteria established by the American College of Radiology. The lesion's configuration is essential for defining the malignancy level of breast lesions [9]. Analyzing the morphology of the lesion is crucial for selecting the most appropriate treatment. The lesion is classified into five groups: regular, lobular, microlobular, irregular, and spiculated, as observed in Figure 1. Zernike polynomials constitute a radial basis. The Zernike basis function is applied to the potential lesion identified in the biomedical image. The gradient magnitudes correspond to the intensity where the region of relevance covered (overlaid) by the disk will be weighted.

Considering the Zernike moment  $z_2^0$ . In the situation in question, the portion of the image under investigation that coincides with the central area of the disk will be examined with the highest intensity due to its scale peak, visualized in Figure 3 by the red color. The maximum intensity is equivalent to the average pixel values in the region, without observing any decrease.

As the analysis expands to the surrounding area of the image, projected onto the disk, the gradient intensity gradually decreases until it reaches the area corresponding to the disk's edge in the image, indicated in Figure 3 by the blue color. Then, in the surroundings of the image area overlapping the disk, there is a gradual decrease in the weighted average of pixel values. The Zernike moment  $z_2^0$  is suitable for regular, rounded lesions, such as cysts.

Figure 4 illustrates an example of anatomical findings being described by the Zernike moment  $z_0^0$ . In contrast, the Zernike moment  $z_5^5$  can describe spiculated lesions. These lesions present lines radiating outward from the center towards the edge, as seen in Figure 3. The American College of Radiology establishes that spiculated lesions indicate a higher probability of malignancy with the characteristic of being a malignant cancer [9]. It is emphasized that many cases observed in clinical practice do not precisely fit the classical image standards and descriptions [15].

A spiculated lesion, although unlikely, may be benign. It is up to the specialist to request a biopsy of the suspicious lesion. Zernike moments play a crucial role in the analysis of lesions in mammograms; however, their applications present some limitations. Zernike moments are sensitive to various factors such as:

The angle of inclination of the anatomical description. Given the heterogeneous nature of breast lesions, they may be positioned at different angles relative to the Zernike moments' disks. This compromises the efficiency in describing the breast lesion.

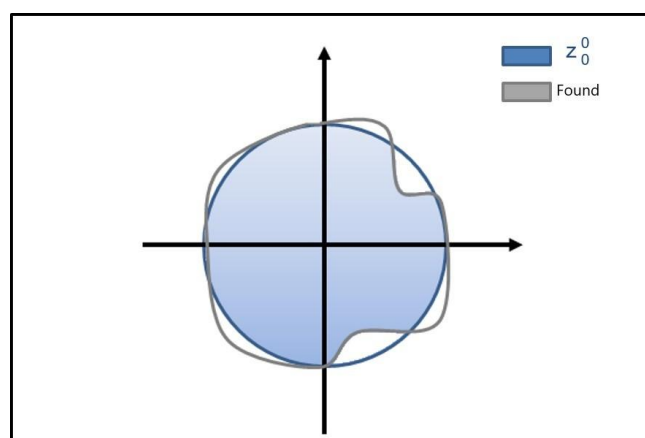
The extent of the area covered by the region of interest in the initial image. Figure 4 highlights that Zernike moments do not incorporate mechanisms to disregard regions that do not encompass zones of interest in the mammogram. This limitation can negatively impact the characterization of the breast lesion.

The non-geometric shape of the anatomical finding also influences the effectiveness of Zernike moments. A non-geometric shape refers to a configuration or pattern that is not precisely defined or described by traditional geometric elements, such as lines, points, or regular figures. As demonstrated in Figure 1, breast lesions can present irregular and asymmetric shapes. In these cases, Zernike moments do not serve as ideal descriptors of the lesions' particularities, revealing inadequacy when faced with this lack of geometric pattern.

Given these considerations, it is evident that, although Zernike moments are valuable for describing lesions in mammograms, their sensitivity to conditions such as inclination, area, and non-geometric shape limits their effectiveness in certain circumstances. These limitations prompt the search for complementary and more robust approaches in mammography analysis to ensure accurate and reliable results.

**Figure 4**

*Description of the shape of the lesion using the Zernike moment  $z_2^0$*



Source: de Lima et al. (2016) [15].

## 2.3 PRELIMINARY STUDIES: NEURAL NETWORKS

Zernike moments have been widely used to extract features related to breast lesions. After the feature extraction stage, pattern recognition of the sample occurs. It is the task of the intelligent algorithm to estimate a diagnosis by comparing the features of the audited biomedical image with those captured during its training stage.

Artificial intelligence algorithms specialize in specific tasks by exploring a vast repository of statistical data. The ability to generalize is acquired by carefully analyzing a representative selection of samples reserved exclusively for the training phase. In the context of pattern recognition, the careful selection of samples that make up the statistical dataset plays a crucial role in the system's effectiveness.

These samples are assigned to classes or labels by a specialized professional or through an automated process conducted by a properly configured instrument. The quality and representativeness of these assignments have a direct impact on the artificial intelligence's ability to correctly identify and classify patterns in new datasets. Therefore, a careful and meticulous approach to the selection and labeling of samples is fundamental to the successful application of artificial intelligence techniques in pattern recognition and similar tasks.

From a set of samples designated as the training set, it is possible to formulate a hypothesis about the various categories associated with the application in focus. Traditionally, these samples undergo an analysis of their features, which are derived from descriptors that capture information on frequency, texture, and shape. After the training

process, it is the responsibility of the artificial intelligence to infer the class of a new sample. This process occurs by comparing the attributes observed in real-time with the patterns stored in the statistical database. During the training phase, seemingly conflicting attributes may coexist simultaneously in the artificial intelligence model, being adjusted and refined to improve its performance.

Advances in artificial intelligence are deeply influenced by biology, with artificial neural networks standing out as one of the most successful techniques. Inspired by the functioning of the human brain, these networks are modeled to simulate biological information processing. Similarly, the initial development of the human brain, especially during the first two years of life, is marked by a rapid expansion of perceptual, cognitive, and motor capacities, reflecting a critical period of learning and development [30].

This learning paradigm serves as a stimulus for numerous researchers seeking to replicate the intricate functioning of the human brain, especially the process of learning through experience. Artificial neural networks are a manifestation of this effort, based on the biological understanding of the human brain [31]. However, unlike a biological brain, where any neuron can establish connections with any other neuron within a certain physical distance, artificial neural networks are structured in discrete layers, with specific connections and defined directionality for data propagation [31].

Regarding classification (categorization), the output layer polarizes the information from the intermediate layer between the application's classes (e.g., cancer patient, non-cancer patient). Neural networks can detect breast cancer in mammography images with an average accuracy of over 98% [12], [13], [14], [15], [16]

When utilizing neural networks, it is crucial to gather a statistically significant number of samples from both the target class and the opposing class. During the training stage, the connections between neurons are adjusted so that the observed features in the target application are represented by a series of adjusted weights.

By adjusting the connections between neurons, the neural network can recognize pre-labeled samples by the specialist, distinguishing between class and counter-class. The learning period is crucial because seemingly unlikely features (input neurons) may occur. For example, it becomes possible to detect a tiny cancer in the mammogram. A specialist supported by a statistical learning machine, such as a neural network, can provide more accurate diagnoses.

After training, the neural network evaluates whether the suspected sample exhibits characteristics more similar to the target class compared to the counter-class(es). In technical terms, the neural network recognizes that a new mammography sample indicates cancer because it exhibits a more distinct pattern than a previously analyzed cancer-free mammogram. In simpler terms, imagine a neural network trained to recognize fruits in images. If we present an image of an apple, it will be correctly identified as an apple because it does not possess characteristics similar to the orange class.

Classical neural networks, also known as shallow neural networks, acquire this name due to their low computational complexity. For this reason, they can operate efficiently on any conventional computer, both during training (learning) and during use.

The training process is completed in just a few minutes due to the reduced number of artificial neurons involved. As a result, the adaptation of the connections between these neurons occurs quickly, even when initialized randomly. During the application phase, the response time of the shallow network occurs in seconds. When well parameterized, shallow neural networks have the potential to achieve accuracies statistically equivalent to any deep learning model [32], [33].

## 2.4 DEEP LEARNING VERSUS SHALLOW NETWORKS

The use of computational methods in biomedical imaging has emerged as an essential strategy to enhance diagnostic reliability by reducing susceptibility to errors. These approaches aim for the automatic identification of anatomical structures related to human anatomy. Inspired by the biological understanding of the human brain, deep neural networks have emerged as key players in this field. These networks, frequently used in pattern recognition in digital images, have achieved remarkable accuracy, driving their application in various tasks.

The term "deep learning" is attributed to these networks due to their high computational complexity. In contrast, classical neural networks, also known as shallow networks, are notable for their lower computational complexity. Deep Learning, as a robust alternative, has solidified its position as the state-of-the-art in overcoming the deficiencies of shallow networks.

Deep Learning techniques, although advanced, impose significant challenges due to computational complexity. The effective implementation of these models requires the use of supercomputers with considerable processing and storage capacity. For instance, Mijwil

(2025) [34] demonstrated the effectiveness of deep convolutional neural networks in the classification of brain tumors from MRI scans. In that study, MobileNetV2 achieved 96.5% accuracy, outperforming other architectures such as DenseNet-201 and Inception-V1. Despite this outstanding performance, the models still operate as black boxes and rely on substantial hardware infrastructure. These challenges justify the search for lighter and more explainable alternatives, such as the extreme learning-based architecture proposed in this study. These robust resources are indispensable for automating the analysis of the entire exploration space, aiming to identify optimal configurations. Thus, the pursuit of diagnostic accuracy using computational approaches not only demands advanced technology but also necessitates the efficient exploration of the vast spectrum of adjustable parameters offered by these techniques.

The development of artificial intelligence specialized in detecting breast lesions in thermograms requires a strategic approach in the choice of learning techniques. In this context, the application of Deep Learning may not be the most viable solution. To illustrate this point, consider the example of the deep neural network Inception-V3, which presents significant complexity with approximately 23.6 million adjustable parameters [35].

This magnitude of parameters requires an equally vast dataset for effective model training. It is relevant to note that Inception-V3 is traditionally trained using the extensive ImageNet database. This database, composed of a variety of generic images, includes objects such as keyboards, mice, and pencils, as well as a diversity of animals, such as lions, elephants, and giraffes, among others. In total, ImageNet contains approximately 1.3 million training images. Thus, there is a training data volume, in the order of millions, that matches the millions of adjustable parameters.

In simple terms, we can say that Deep Learning is data-hungry—a large number of adjustable parameters must be fed with a proportionally extensive amount of input data. In the context of biomedical engineering, it is crucial to consider that the availability of thermograms may be limited. It is important to highlight that Deep Learning demonstrates its maximum potential in situations where there is an abundance of training data, allowing the network structure to acquire the generalization capability necessary to handle a variety of scenarios. However, when faced with a limited dataset, composed of hundreds rather than millions of samples, the generalization capability of Deep Learning can be compromised.

In the case of artificial intelligence aimed at detecting breast lesions in thermograms, the use of Deep Learning may initially seem like an attractive choice, but there are some

points to consider. Imagine that Deep Learning is like a powerful race car that needs a wide, obstacle-free road to show its full potential. However, if the road is full of tight turns and obstacles, this car might not be the best option. In the context of biomedical engineering, Deep Learning is like this race car. It needs a large amount of data to function correctly—it's as if it has an insatiable appetite for data. If we do not have a vast amount of data available, the performance of Deep Learning can be compromised.

While Deep Learning proves highly effective in contexts where there is an abundance of data, for artificial intelligence specialized in thermograms, other approaches, such as supervised learning techniques with smaller and more focused datasets, may be more appropriate and efficient. These approaches can offer a more practical and effective alternative for developing solutions tailored to breast lesions in thermograms.

One disadvantage of deep networks is the long training time. Adjusting synaptic weights with gradient-based iterative methods is computationally expensive. Even using a computer with very high processing speed and large memory capacity, basic training of a deep network could take months or even years. The latest generation of neural network methods requires the use of large datacenters instead of relying on conventional desktop computers. These methods may depend on millions of adjustable (trainable) parameters.

Moreover, deep networks have limited parallel processing capacity due to the sequential nature of convolutional layers. Each layer is processed only after the completion of the previous layer. In a situation where all layers were executed simultaneously, the producer-consumer paradigm would occur. The consumer layer could attempt to read data while the producer layer is still processing them, potentially resulting in premature and incorrect data acquisition [36].

There are deep network models that attempt to process data simultaneously, but they are in the early stages of development and have not yet demonstrated high levels of accuracy in various applications [37], [38]. The deep network proposed by dos Santos et al., 2019, is parallelizable and has 30,000 convolutional filters activated simultaneously. When run on a powerful server, the developed network shows a training time comparable to that of shallow networks. As long as it is on a server, this model shows a training period not discrepant from shallow networks.

The aforementioned deep network shows excellent results when applied to image processing, particularly in optical character recognition [38]. However the parallelizable deep network proposed by SANTOS et al. (2019) did not succeed when applied to malware pattern

recognition. Its results were statistically inferior to both shallow networks and deep networks based on sequential layers (cascade graphs) [37]. Therefore, there is no evidence that a parallelizable deep network achieves good results in the field of biomedical engineering.

A computational technique based on deep learning may suffer from the curse of dimensionality. For example, the deep network Inception-V3 has 23.6 million adjustable parameters [35]. It is impractical to infer which of these millions of adjustable parameters can optimize the network's accuracy. It also becomes unfeasible to try to formulate an explanation of how a deep network works. For instance, there is no way to know which parameters control the decision boundary in relation to the target classes of the application. In summary, some deep networks function as black boxes with little control and/or explanation of their actions.

Transfer learning emerges as an ingenious strategy to circumvent the extensive time demands associated with deep network training. Instead of starting with a blank slate, devoid of knowledge or skill, the transfer learning approach introduces a more advanced starting point. The deep network, previously trained for various tasks, is repurposed, functioning as a precursor, bringing with it a wealth of information accumulated during its prior iterations.

This prior knowledge, although originally intended for a different application, is adapted and refined for the new task at hand, allowing for a rapid acceleration of the training process. Thus, the period required to train a deep network, which would previously demand months of dedication, is drastically reduced to just a few days, thanks to the inheritance of prior learning. This smart transition enhances training efficiency, maximizing the network's potential and paving the way for a faster and more precise adaptation to the specific demands of each application. However, even with this significant reduction in training time, there remains some hesitation in adopting deep networks, especially in the field of biomedical engineering.

This occurs due to the need to convince managers and professionals in the field of the effectiveness and reliability of these models. Gaining the support of managers to wait days until the artificial intelligence completes its learning and is ready to make predictions is not a simple task. Therefore, despite the benefits of transfer learning, it is important to address and overcome these concerns to promote a broader and more effective adoption of these technologies.

A new approach to transfer learning has emerged to address the need to reduce training time in deep networks. This emerging alternative has stood out as the state-of-the-art in intelligent computing and finds application in various fields. Through this additional

strategy, a scientific study can acquire the prestige associated with Deep Learning, while being completed in a time comparable to that of less complex networks.

A deep network, previously trained for different purposes, retains its trainable parameters unchanged. Functioning as a combination of a feature extractor and a data miner, the deep network receives data from the specific problem and produces its own output neurons, which were trained for another application. For example, the deep network Xception was developed with a specialization in identifying objects and organisms in images.

The Inception-V3 is capable of categorizing images into 1,000 distinct classes, including objects like keyboard, mouse, pencil, as well as various animals such as lion, elephant, and giraffe, among others. Undoubtedly, the Inception-V3 significantly contributes to the reputation of deep networks, demonstrating a remarkable generalization capability. In transfer learning, the 1,000 output neurons of the Inception-V3, previously trained for other purposes, can be used as input for a shallow classifier. In this way, the shallow classifier can recognize patterns in the target application, even without having direct access to its data.

In legal and biomedical domains, transfer learning between deep and shallow networks faces significant resistance in its adoption. Artificial intelligence might recommend the conviction of a defendant because their court case "matches" a pattern; 1.1% with an image of a lion, 1.5% with a photo of a keyboard among the 1,000 output categories in a cutting-edge deep network. The deep network thus functions as an arbitrary data miner and feature extractor. It would also not be trivial to convince a healthcare professional that a patient has cancer because the image "matches" a pattern 1.3% with an image of a giraffe among the 1,000 output categories of a deep network.

Several conjectures and theories attempt to rationally explain the high accuracy rates achieved by applying transfer learning between deep and shallow networks. One possibility is that during the extensive training periods of deep networks, excellent quality frequency, texture, and shape descriptors are developed. These descriptors would be integrated into the millions of adjustable parameters of a deep network architecture. It becomes practically impossible to computationally identify which are these spontaneous descriptors and where exactly they are located within the structure of the deep network. However, it is plausible that these spontaneous descriptors of frequency, texture, and shape could be useful in various applications, regardless of the purpose for which the deep network was originally trained.

Preliminary Studies: Extreme Learning Machines.

In most neural networks, such as MLP (Multi-Layer Perceptron) [39], it is crucial to understand the network elements to achieve the best performance in solving the problem. A common concern in this type of structure is avoiding being trapped in local minima, making it essential to incorporate control mechanisms to escape these situations. Another typical characteristic of this type of network is the extensive training time required for the network to perform accurate classifications.

On the other hand, in the Extreme Learning Machine (ELM), it is not necessary to increase the number of adjustable parameters, such as the learning rate commonly used in neural networks based on backpropagation. This technique stands out for its speed in training and data prediction compared to other classifiers.

ELM is a single hidden layer and non-iterative network. Its learning model is based on the Moore-Penrose pseudoinverse, where the weights between the hidden layer and the output layer are calculated [40], [41]. ELM training is performed in a batch mode, where all data is presented to the network before the weights related to the synaptic connections between the neurons of the hidden and output layers are adjusted. The learning process of the ELM consists of a single iteration. In summary, there is no data backpropagation; therefore, ELM does not face overfitting problems.

Due to its single iteration, ELM training is faster compared to traditional methods. Moreover, since it does not use the gradient descent method and does not require setting a learning rate parameter, the ELM network simplifies the training process, eliminating the need for manual adjustments and making it less prone to configuration errors.

Mathematically, in the ELM network, the input attributes  $x_{it}$  correspond to the set  $\{x_{it} \in \mathbb{R}; i=1, \dots, n; t=1, \dots, v\}$ . There are  $n$  features extracted from the application and  $v$  training data vectors. The hidden layer  $h_j$  consisting of  $m$  neurons, is represented by the set  $\{h_j \in \mathbb{R}; j \in \mathbb{N}^*; j = 1, \dots, m\}$ . ELM training is efficient due to its simplified structure, requiring few steps. Initially, the input weights  $w_{ji}$  and bias:  $b_{jt}$  are chosen randomly. Given an activation function  $f: \mathbb{R} \rightarrow \mathbb{R}$ , learning occurs in three distinct steps:

Random generation of the weight  $w_{ji}$ , corresponding to the weights between the input and hidden layers, and bias:  $b_{jt}$

Calculation of the matrix  $H$  which is equivalent to the output of the neurons in the hidden layer.

Calculation of the output weight matrix  $\beta = H^\dagger Y$ , where  $H^\dagger$  is the Moore-Penrose generalized inverse of matrix  $H$ , and  $Y$  corresponds to the desired output matrix, where  $\{Y_{tc} \in \mathbb{R}; t = 1, \dots, v; c = 1, \dots, \zeta\}$ .  $\zeta$  is the number of classes (e.g., benign, cyst).

The concept of an inverse matrix is related to the identity matrix  $I$ . An original square matrix  $H$  multiplied by its inverse  $H^{-1}$  equals the identity matrix,  $H \cdot H^{-1} = I$ . However, in cases where the matrix has a rectangular dimension, and thus is not square, an approximately inverse matrix  $\cong H^{-1}$  is generated. This approximately inverse matrix is responsible for polarizing the synaptic weights between neurons. The pseudo-inverse matrix  $H^{-1} \cong H^\dagger$  pushes the synaptic weights from the decision boundary towards the extremes (poles) of the secondary diagonal.

Mathematically, the pseudo-inverse matrix  $H^\dagger$  uses the singular value decomposition  $H = U \Sigma V^*$ , where  $U$  is a real or complex unitary matrix of size  $n \times n$  and  $n$  is the total number of input neurons.

$\Sigma$  is a rectangular diagonal matrix of size  $n \times \sigma$  with non-negative real numbers on the main diagonal;  $n$  is the total number of input neurons, and  $\sigma$  is the total number of training data vectors.  $V$  (the conjugate transpose of  $V$ ) is a real or complex unitary matrix of size  $\sigma \times \sigma$ . The diagonal entries  $\Sigma_{it}$  of  $\Sigma$  are called the singular values of  $H$ . The  $n$  columns of  $U$  and the  $\sigma$  columns of  $V$  are the left singular vectors and the right singular vectors of  $H$ , respectively. The pseudo-inverse of  $H$  is then equal to  $H^\dagger = V \Sigma^{-1} U^*$ .

The output of the neurons in the hidden layer, represented by the matrix  $H$ , is obtained using the kernel  $\phi$ , inputs, and hidden layer weights, as shown in Eq. (3). The kernel  $\phi$ , inputs, and weights of the dataset between the input and hidden layers are employed. The output weights  $\beta$  and the desired output matrix  $Y$  are described in Eq. (4) and Eq. (5), respectively.

$$H_{tj} = \begin{bmatrix} \phi_1^1 & \phi_2^1 & \dots & \phi_v^1 \\ \phi_1^2 & \phi_2^2 & \dots & \phi_v^2 \\ \vdots & \vdots & \ddots & \vdots \\ \phi_1^m & \phi_3^m & \dots & \phi_v^m \end{bmatrix}_{m \times v} \quad (1)$$

$$\beta_{jc} = \begin{bmatrix} \beta_1^1 & \dots & \beta_\zeta^1 \\ \beta_1^2 & \dots & \beta_\zeta^2 \\ \vdots & \ddots & \vdots \\ \beta_1^m & \dots & \beta_\zeta^m \end{bmatrix}_{m \times \zeta} \quad (2)$$

$$Y_{tc} = \begin{bmatrix} y_1^1 & \dots & Y_\zeta^1 \\ y_1^2 & \dots & Y_\zeta^2 \\ \vdots & \ddots & \vdots \\ y_1^v & \dots & Y_\zeta^v \end{bmatrix}_{v \times \zeta} \quad (3)$$

The learning model of ELM networks is based on the use of kernels, which are essentially mathematical functions employed as a fundamental method for the development of ELM neural networks. In its standard configuration, the kernel refers to the linear function, aimed at achieving efficient linear separation of the data. Equation (6) describes the Linear kernel  $\varphi$  of an ELM network. The function is defined in terms of  $\varpi$  (  $x_{t,1 \dots n}$  ;  $w_{1 \dots m, 1 \dots n}$  ;  $b_{1 \dots m, t}$  ) .

$$\varphi_t^j(\varpi) = x_{ti} \cdot w_{ji} + b_{jt} \quad (4)$$

An essential issue concerning extreme neural networks is to ascertain the correlation of the dataset as a function of the random generation of weights between synaptic layers.

Achieving pertinent results in a specific application with a random weight generation seed does not imply that the same seed, when applied in a different scenario, will yield adequate results. Identifying the optimal seed for random weight generation is a challenge that may require an extensive period. Exhaustively exploring the search space becomes computationally unfeasible.

A frequently employed option involves multiple executions of a single neural network structure. In each execution, different techniques are applied to generate initial random synaptic weights. This approach allows for the assessment of whether variations in initial synaptic weights can significantly impact the results. At the end of the experiments, a high standard deviation would indicate dispersion in the results. Consequently, the neural network would be subject to influences and correlations with the random initial conditions.

In such a situation, the initial conditions could abruptly degrade or enhance the neural network's accuracy. Implementing a solution with such a characteristic in clinical practice, for example, would be precarious. During the utilization phase, a slight alteration in patient profiles could result in a sudden deterioration in the results provided by the computational solution. The neural network would only be effective for cases statistically similar to those presented during training. It is noteworthy that numerous cases observed in clinical practice do not precisely align with traditional images and descriptions [15].

## 2.6 THERMOGRAPHY

Thermography is an imaging technique that utilizes infrared (IR) radiation emitted by objects to create visual representations of temperature variations. This technique is based on the emission of IR radiation by objects with a temperature above absolute zero, which is captured by a specialized detector and processed to generate a thermographic image. In this image, different colors or shades represent different temperatures, following a color scale where warmer colors indicate higher temperatures, and cooler colors indicate lower temperatures.

The acquisition of thermographic images is performed using thermographic cameras, which capture the IR radiation emitted by the object and process it to generate the thermographic image. This technique offers several advantages, such as the detection of thermal anomalies that are not visible to the naked eye, the non-destructive nature of the measurement, and the efficiency in analyzing temperature variations in real-time.

However, interpreting thermographic images can be complex and requires specialized training, in addition to the relatively high cost of thermographic cameras. Furthermore, there are environmental limitations that can affect the accuracy of measurements, such as lighting conditions, atmospheric variations, and extreme weather conditions. In particular, the presence of wind, rain, fog, or direct sunlight can interfere with the quality of thermographic measurements.

Despite these limitations, thermography remains a valuable tool in various applications, including predictive maintenance, medical diagnostics, building inspections, and more. Figure 5 shows the equipment that was used to produce the thermographic images in this work's database

**Figure 5**

*Mechanical apparatus used in the acquisition room. In (1) are the rails used to move the camera support (2) towards the patient, positioned on the swivel chair shown in (3); the bars in (4) are used to position the arms during the examination*



Source: Santana et al. (2018) [42].

## 2.7 DEVELOPMENT

**Figure 6**

*Development details*

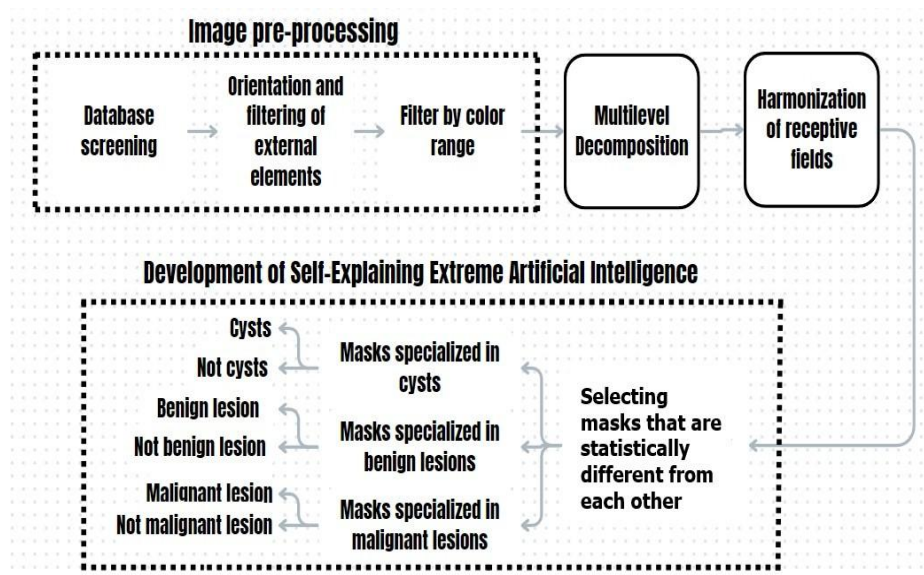


Figure 6 illustrates the block diagram, which details each of the stages in the development process. This diagram provides a comprehensive and enlightening view of the workflow adopted.

## 2.8 PROCESSING OF THERMOGRAPHIC IMAGES

In order to extract the necessary information from the images, it is essential to preprocess the database, as this involves a self-explanatory artificial intelligence model. Raw data cannot be directly utilized with the expectation that the algorithm will correctly interpret them. Therefore, prior data manipulation is necessary so that the program assimilates only the relevant information. The preprocessing can be explained by dividing it into stages.

### 2.8.1 Database Screening

An evaluation of the entire dataset, comprising 1,052 thermographic images, is conducted. These images are categorized based on their diagnoses, which include Cyst, Benign Lesion, Malignant Lesion, and Absence of Lesion. Each diagnostic type contains multiple images, varying in their orientations. In other words, the thermographic images were acquired from various distinct perspectives to facilitate the identification of lesions.

Figure 7 displays thermographic images sourced from the employed database. Classical descriptions often point to abrupt variations in heat intensity between benign and malignant lesions. In the academic literature, a malignant lesion is expected to exhibit a much higher heat intensity compared to a benign lesion or a cyst.

However, this is often not the case in the image dataset derived from clinical practice. The cases, as shown in Figure 7 present very close heat intensities, even with different diagnoses. The discrepancy between the results obtained in clinical practice and those described in the academic literature makes breast cancer diagnosis in thermograms a complex task, even for experienced specialist professionals.

## 2.9 SELECTION OF ORIENTATIONS AND FILTERING OF EXTERNAL ELEMENTS

In this stage, the images undergo a new categorization process. In the previous stage, the goal was to catalog the images according to their diagnosis: malignant lesion, benign lesion, no lesion, and cyst. In the current stage, the objective is to catalog the images based on their orientation.

The database includes eight orientations: LSRB (Left Side; Right Breast), LSLB (Left Side; Left Breast), RSLB (Right Side; Left Breast), RSRB (Right Side; Right Breast), RB (Right Breast), LB (Left Breast), T1 (Torso), and T2 (Torso).

Due to the variety encountered in clinical practice, it is necessary to select certain orientations over others to promote a more coherent and uniform approach to image

categorization. In this database, for example, an MD image of a patient with a cyst does not guarantee that the cyst is located in the right breast. The cyst could be in the left breast, and therefore outside the image. Additionally, there is no guarantee that the patient underwent all eight orientations.

Thus, it is not possible to make deductions and inferences, as the lesion causing the diagnosis may be outside the image. Moreover, there may be no corresponding image elsewhere in the entire database. Therefore, only the T1 orientation is considered in the present study. The rationale is that the representation of the patient's torso maximizes the chances that the lesion is contained within the image.

Within the dataset in question, there were images containing elements irrelevant to the analysis. These elements included initial information directly from the medical device, such as ambient temperature, date, time, and the image's color map, among others. These pieces of information were inserted during the image capture stage. Additionally, parts of the arm, abdominal region, and even objects from the surrounding environment, which had no correlation with the region of interest, were observed.

For example, parts of the chair and/or backrest overlapped with the breast in several images from the database. To improve the quality of the dataset, it was crucial to carry out a meticulous cropping process, focusing specifically on the area of interest in each image. This procedure was adopted to eliminate any components that were redundant or irrelevant. The objective is to maximize the likelihood that only the essential elements for analysis and diagnosis remain present in the images.

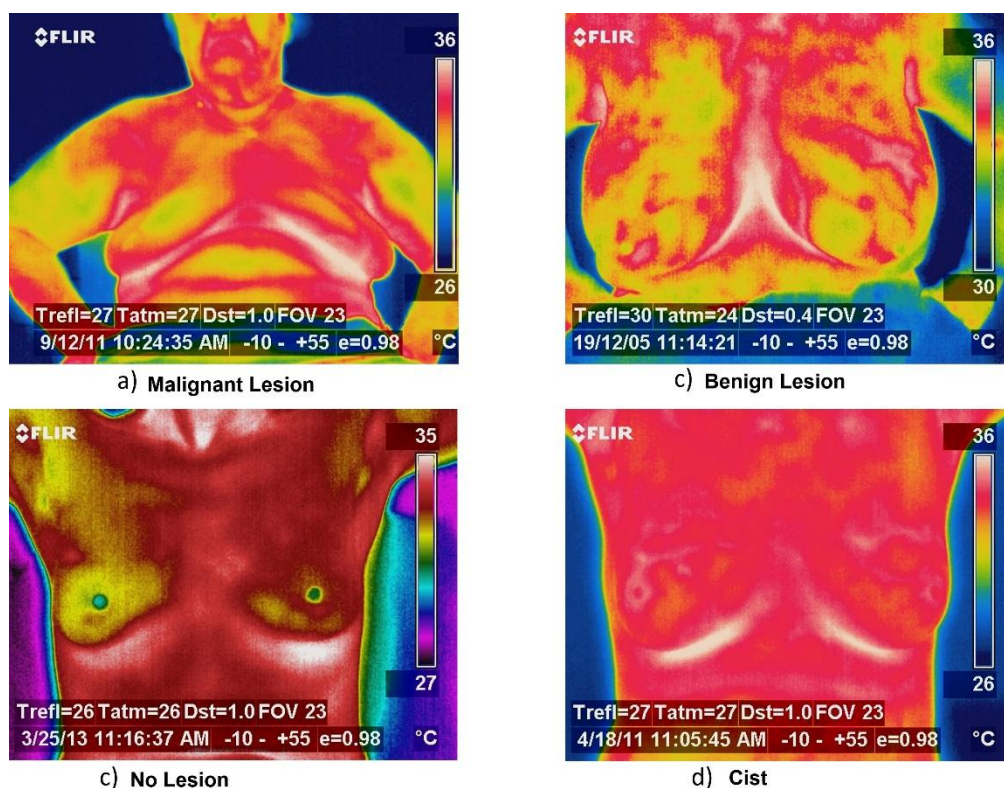
### 2.9.1 Color Range Filtering

Figure 8 illustrates the process of color range filtering. The Euclidean distance is calculated between each pixel of the cropped image and the previously determined color spectrum. The custom color spectrum is composed of eight ranges: dark purple, light purple, dark blue, light blue, green, yellow, red, and white.

Figure 8 illustrates the process of color range filtering. The Euclidean distance is calculated between each pixel of the cropped image and the previously determined color spectrum. The custom color spectrum is composed of eight ranges: dark purple, light blue, green, yellow, red, and white.

**Figure 7**

*Database screening*



In the color range filtering process, only the pixels within the yellow to white range are retained. The remaining pixels are incorporated into the background. These regions are interpreted as being cold areas consistent with the patient's metabolism. Therefore, no lesions or cysts are present in these low heat intensity regions.

After removing the cold regions from the image, it becomes possible to identify the area of the image associated with the region of interest. Color range filtering is fundamental to the proposed technique. This filtering method effectively eliminates non-interest regions such as the arms, neck, and pectoral muscles. It should be noted that horizontal cropping and final adjustments were performed manually.

## 2.10 MULTILEVEL IMAGE DECOMPOSITION

In this study, we propose the decomposition of thermographic images. The image decomposition process occurs at different levels (resolutions). Initially, there is a focus on studying the lesions and their sizes. In more advanced levels, only smaller findings remain. During the

decomposition process, there is a loss of resolution due to the blurring of the image at each level. This occurs because, during decomposition, larger bodies are smoothed and merged into the background of the image. Size analysis is critical in breast lesions since breast carcinoma can be detected in both very small lesions and lesions that encompass almost the entire breast.

To perform the proper decomposition of the images, the thermogram is converted to grayscale. This transformation suppresses information related to hue and saturation, retaining only the luminosity component. This procedure was

adopted to simplify image manipulation by eliminating characteristics that were not pertinent to the analysis. The image is decomposed considering the texture and illumination of each threshold. The contrast of the image is modified at each level. The process draws inspiration from the fuzzy c-means technique, which is essentially a clustering algorithm that assigns data points to clusters based on their similarity.

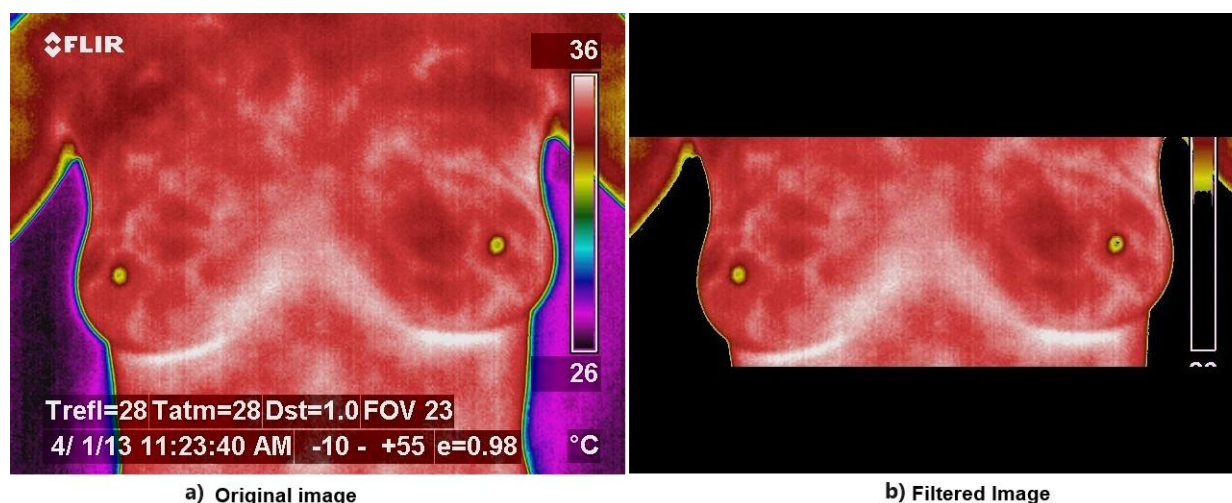
The custom decomposition is used to group adjacent pixels in the image that have similar values. The proposed decomposition method is also inspired by wavelet series to

represent the image at multiple levels. Breast lesion detection can be achieved by decomposing the thermogram into multiple levels. The state-of-the-art typically decomposes the mammogram into only two levels using MALLAT wavelets [43].

However, in the proposed methodology, the image is decomposed until saturation occurs. This choice is based on the understanding that breast cancer does not have a predefined shape or size, making it essential to study all elements within the region of interest until they are fully delineated. It is considered that decomposition into two levels, as proposed by the state-of-the-art, is insufficient to segment all the elements present in the region of interest in biomedical images. The complexity of breast lesion characteristics requires a more in-depth approach to ensure comprehensive and precise segmentation.

**Figure 8**

*Removal of external elements from the patient*



Computational solutions applied to biomedical images, such as in the detection of *Aedes Aegypti* eggs (vector of dengue) and *Schistosoma* (transmitter of schistosomiasis), involve dimensions that are not significantly different from each other. In such contexts, the decomposition of the original image into multiple levels would not be necessary. However, when dealing with breast lesions, multilevel decomposition is essential. Breast lesions do not follow a predictable size pattern, ranging from fractions of centimeters to occupying almost the entire breast. Therefore, the decomposition of breast lesions in thermograms is crucial since the initial levels focus on studying heat maps over a broad area, while the final levels allow for the analysis of small-scale heat maps.

Figure 9 exemplifies the decomposition of the thermogram into various levels, culminating in its saturation. Benign and malignant lesions generally occupy the region of highest temperature in the area of interest, characterized by red and white color spectra. However, this phenomenon can inadvertently highlight elements unrelated to clinical interest. A common example is observed in patients with adipose breast tissue, where a heat area may appear between the breast and the pectoral muscle, not corresponding to a legitimate breast lesion, as seen in Figure 7 (a). Thus, it is crucial to employ pattern recognition techniques to differentiate between genuine breast lesions and false positives associated with areas of increased temperature.

In the proposed methodology, the pattern recognition phase of lesions is performed after image processing. Each element in the region of interest contributes to forming a receptive field capable of identifying potential tissue anomalies.

Conversely, Figure 10 presents the decomposition of the remaining cold regions. Reverse decomposition is important for studying breast cysts since, as a general rule, they occupy a cold region in the area of interest. In computational terms, the spectrum range of breast cysts varies between yellow and red colors. In multilevel decompositions, the legend presents the letter *n* accompanied by a value. When a direct value is subtracted from an image in MATLAB, each pixel of the image is affected by the subtraction of the specified value. This can produce different effects depending on the chosen value and the type of image.

Initially, if the subtracted value is positive, the image generally darkens as each pixel's value is reduced by the specified amount. On the other hand, if the subtracted value is negative, the image tends to lighten as each pixel's value increases by the absolute value of the specified amount.

It is important to note that the pixel values of the image are typically represented as 8-bit integers (0 to 255) or normalized floating-point values between 0 and 1. If the result of the subtraction is less than 0 for an 8-bit image, for example, the negative values will be truncated to 0, which can result in a loss of detail in the darker areas of the image.

Moreover, depending on the chosen value for subtraction and the dynamic range of the image, there may be a loss of information or detail after the operation. If the subtracted value is too large compared to the pixel values in the image, details in the darker regions may be lost. Similarly, if the added value is too large compared to the pixel values in the image, details in the darker regions may be lost due to the compression of pixel values toward white.

**Figure 9**

*Multilevel decomposition*

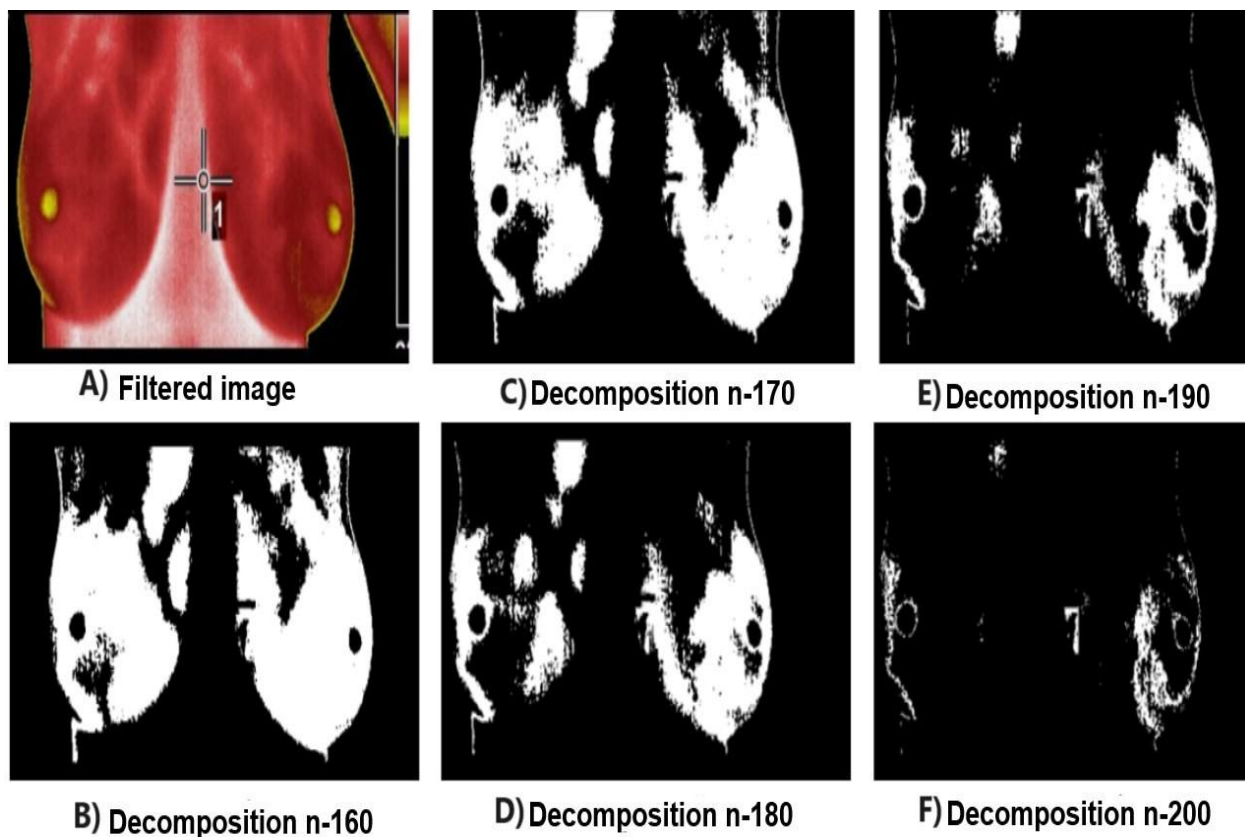
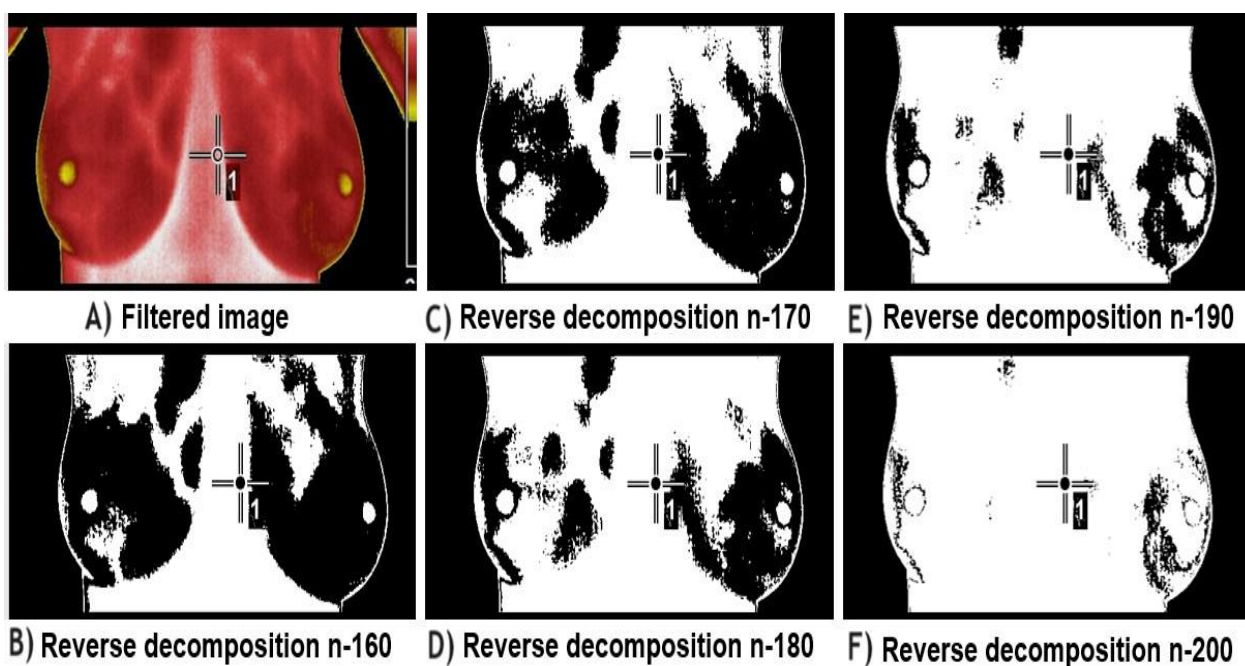


**Figure 10**

*Reverse multilevel decomposition*



### 2.10.1 Harmonization of Receptive Fields (Masks)

The result of the decomposed image consists of rough, defective, and unintelligible images with abrupt cuts. The anatomy of the human body does not manifest itself in an idealized manner. Patients, for instance, may have twisted and uneven breasts. If these images were presented to a physician, it is very likely that they would believe that the artificial intelligence failed to detect any relevant information in the image. Therefore, it is essential to harmonize the "masks" in order to fill internal noise and smooth the edges, bringing the already grouped elements closer to the idealized images found in radiology textbooks.

After decomposing the images, several images containing the extracted elements were generated. To distinguish these elements, programming functions were employed, allowing adjacent pixels to be grouped into one figure, while other groups were separated into different figures. These elements were later used for the creation of the "masks."

Figures 11 and 12 display the "masks," which are the result of the harmonization of the decompositions derived from the image gradient. This implies that, after decomposition, the color scale is readjusted to make abrupt transitions more comprehensible and visually acceptable. In order to extract the maximum amount of information from this harmonization, the figures are progressively enlarged, thus generating new "masks."

**Figure 11**

*Receptive fields, one color band*

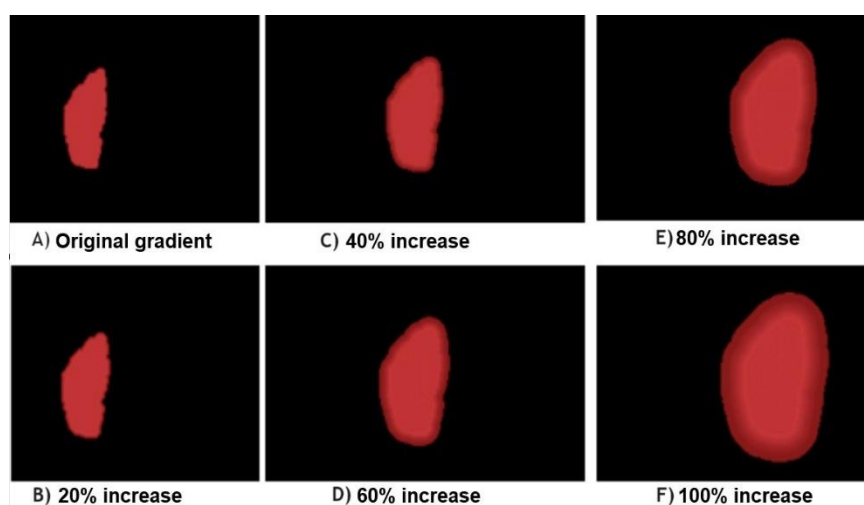


**Figure 12**

*Receptive fields, two color bands*

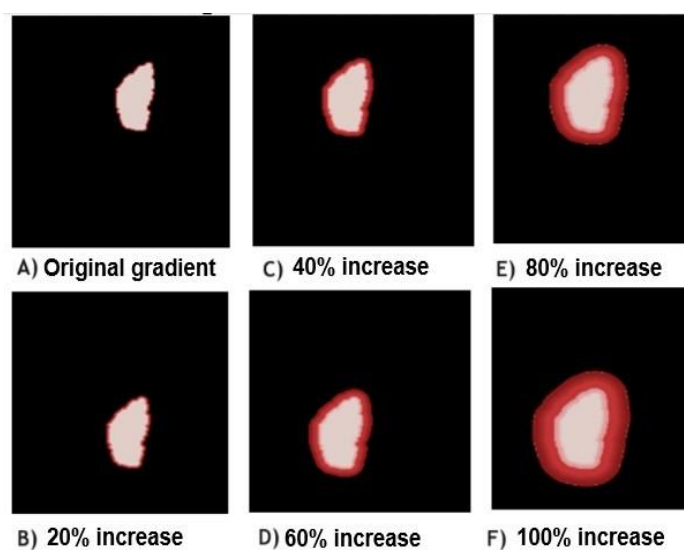
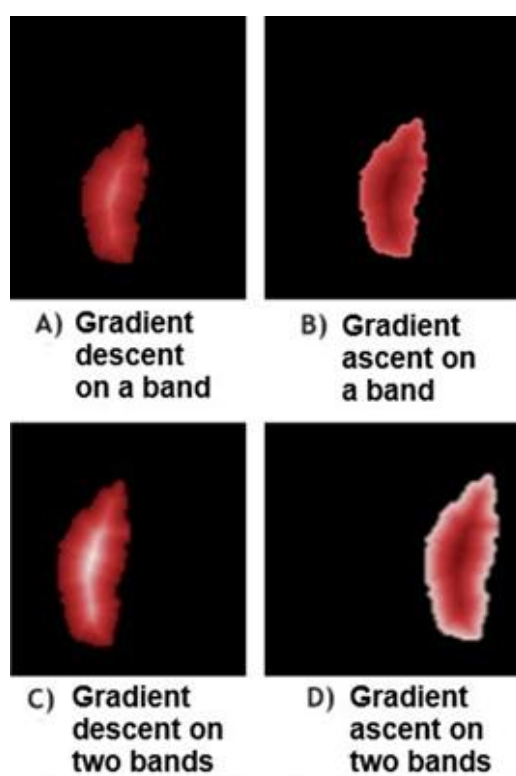


**Figure 13**

*Receptive fields masks*



## 2.11 DEVELOPMENT OF EXTREME SELF-EXPLANATORY ARTIFICIAL INTELLIGENCE

When performed by shallow neural networks, the pattern recognition stage is dependent on the feature extractors of the samples. Due to their low computational complexity, shallow networks lack mechanisms to convert the samples into a repository of statistical learning. When employing shallow networks, the task of detecting and classifying breast lesions is highly dependent on the feature extraction stage [15].

In the state-of-the-art, Zernike moments have been widely used to extract features related to the shape of breast lesions. The shape of the lesion is essential for determining the malignancy grade of breast lesions [12], [13], [14]. Zernike moments are capable of describing the evaluated lesion according to the American College of Radiology guidelines. The study of the lesion shape is necessary for selecting the appropriate treatment. A regular lesion has benign characteristics, while a spiculated lesion is usually malignant [9].

The Zernike method involves radial basis polynomials. The Zernike basis function is projected onto the finding, a potential tumor, present in the biomedical image. The gradient values, in scale, correspond to the intensity with which the region of interest covered (overlaid) by the disk will be evaluated. The scales determine the intensity with which the image region under study, covered (overlaid) by the disk, will be evaluated.

Consider, for example, the Zernike moment  $z_{2^0}$ . In this case, the region of the image under study, overlaid on the central region of the disk, will be evaluated with maximum intensity because it has a peak scale, represented in Figure 3, through the red color. Maximum intensity corresponds to the average of the pixel values in the region without any decrease. As the peripheral region of the image, projected onto the disk, is studied, the gradient intensity decreases until it reaches the area of the image corresponding to the disk's edge, represented in Figure 3, through the blue color. Thus, in the peripheral region of the image overlaid on the disk, there is a weighted average, corresponding to a decrease in the pixel values. The Zernike moment  $z_{2^0}$  is suitable for regular, round-shaped lesions, such as cysts. Figure 4 shows an example of an anatomical finding being described by the Zernike moment  $z_{0^0}$ .

In mammography images, the Zernike moment  $z_{5^5}$  can describe spiculated lesions. These lesions have radiating lines extending from the center to the periphery, as seen in Figure 3. The American College of Radiology establishes that spiculated lesions correspond to the highest degree of malignancy in terms of the characteristics of malignant cancer [9]. It is emphasized that many cases seen in clinical practice do not fit precisely into the classic

images and descriptions [15], [44]. A spiculated lesion, although unlikely, can be benign. It is up to the specialist to request a biopsy of the suspicious lesion.

Although Zernike moments are fundamental in characterizing lesions in mammograms, their sensitivity to variables such as inclination, area, and non-geometric shapes imposes limitations on their effectiveness in specific scenarios. These restrictions prompt the need to seek supplementary and more robust approaches in mammogram analysis. The goal is to ensure that the results can be rationally presented to a specialist.

Unlike Zernike moments, the present work creates authorial receptive fields. The receptive fields are harmonized versions derived from the decomposition of the region of interest of the raw sample. Instead of preconceived geometric surfaces, harmonized versions of the thermogram compatible with a probable lesion are generated.

The success of authorial receptive fields can be attributed to their ability to model any breast lesion or cyst. The mapping made by the authorial receptive fields does not adhere to preconceived geometric surfaces like the Zernike moments. Authorial receptive fields naturally detect and model the regions of breast lesions and cysts. Since they are created from elements extracted from the thermogram itself, the authorial receptive fields naturally handle the detection and classification of the shapes of bodies present in the thermogram. The modeling capability of human anatomy, such as twisted, asymmetrical, and uneven breasts, is emphasized.

Through authorial receptive fields, it becomes possible to formulate a self-explanatory hypothesis regarding the presence of a breast lesion or cyst. The extreme neural network is employed to recognize the pattern of the anatomical anomaly. Extreme neural networks are computational intelligence models with learning capabilities that allow for the creation of data mappings without backpropagation. Extreme neural networks are computationally very simple but can provide excellent accuracies [15]. As an advantage, it is feasible to explain extreme learning to a human due to the low volume of calculations. It would become possible to convince the specialist that the tool can provide an adjusted and useful "second opinion". There is an establishment of a correlation between the receptive field and the proposed extreme neural network architecture. The input attributes  $x_{it}$  relate to the decomposed region of the raw thermogram and are temporarily covered by the receptive field.

The input attributes  $x_{it}$  correspond to the set  $\{x_{it} \in \mathbb{R}; i = 1, \dots, n; t = 1, \dots, v\}$ . There are  $n$  features extracted from the application, where  $n$  is the number of pixels in the decomposed region of the raw thermogram, and  $v$  is the training data vector.

To adjust the dimensions, the receptive field is resized based on the input attributes. After resizing, the pixels contained in the receptive field correspond to the weights  $w_{ji}$  associated with the synaptic connections between the input layer and the hidden layer. The hidden layer  $h_j$ , consisting of  $m$  neurons, where  $m$  corresponds to the number of pixels in the receptive field. The hidden layer  $h_j$  is represented by the set  $\{ h_j \in \mathbb{R}; j \in \mathbb{N}^*; j = 1, \dots, m \}$ . Next, the output weight matrix  $\beta = H^\dagger Y$  is calculated, where  $H^\dagger$  is the Moore-Penrose generalized inverse matrix of matrix  $H$ , and  $Y$  corresponds to the desired output matrix, where  $\{ Y_{tc} \in \mathbb{R}; t = 1, \dots, v; c = 1, \dots, \zeta \}$ .  $\zeta$  is the number of classes (e.g., target class, counter-classes).

The original formulation of the extreme neural network involves the random generation of weights, which differs from the approach of this self-explanatory artificial intelligence proposal. The idea of generating random neurons is discarded since the architectural structure itself provides the foundation for explaining the diagnosis offered by the "second opinion" tool.

The learning process of the extreme network is based on a kernel. This type of learning enables the recognition of the anatomical finding's pattern without the need to increase the number of adjustable parameters. Equation (7) describes the authorial kernel concerning the processing of the first neuron in the hidden layer. It involves the mean squared error between the input attributes  $x_{it}$  and the synaptic weights  $w_{ji}$ .

$$\varphi_t^1 = (1/n) \sum_{i=1}^n (x_{it} - w_{ji})^2 \quad (7)$$

The masks and decomposed images are all in our authorial repository: [45].

Figure 14 displays the operation of an authorial receptive field. Figure 15 presents a QR code that redirects to a video on YouTube demonstrating the functioning of the authorial artificial intelligence. It is important to note that the authorial field fits into the decomposed region of the thermogram with the greatest affinity and, consequently, the lowest mean squared error. Unlike Zernike moments, authorial receptive fields have the ability to decompose without exceeding the boundaries of the target region in the thermogram. During execution time, the receptive fields undergo self-remodeling to reduce the mean squared error in relation to the decomposed region of the thermogram. This self-remodeling occurs in terms of shape and rotation.

As described in Equation (8), the second neuron in the hidden layer corresponds to the number of pixels in the intersection of the decomposed region of the thermogram and the self-remodeling receptive field.

$$\varphi_t^{j2} = (1/n) \bigcap_{i=1}^n (x_{it}, w_{ji}) \quad (8)$$

From the third to the thirty-fourth neuron, there is feature extraction related to the shape and texture of the self-remodeling receptive field. These neurons are detailed in the Appendices. In the current artificial intelligence approach, pattern recognition related to breast lesions takes into account the local information specified by these initial neurons.

The artificial intelligence also incorporates global information from the thermogram, considering its overall heat map. From the thirty-fifth neuron onward, the extraction of the authorial color spectrum, composed of 9 (nine) bands, takes place. The first band is dedicated to regions preliminarily eliminated, as described in subsection 4.1.2. Additionally, there are 8 (eight) bands in the authorial spectrum: dark purple, light purple, dark blue, light blue, green, yellow, red, and white. This spectrum is defined in subsection 4.1.3.

The Eq. (9) describes the processing from the second to the ninth neuron. These neurons correspond to the color spectrum.  $S \rightarrow \{0,255\}$  is the thermogram in the form of a matrix such that  $S \in \mathbb{N}^2$ .

$$\varphi_t^{j+35} = \sum_{j=1}^9 s_j \quad (9)$$

## 2.12 THE IMPORTANCE OF SELF-EXPLAINABLE ARTIFICIAL INTELLIGENCE

This work argues that it is not enough for computational techniques to simply operate correctly; the mechanisms must also be capable of explaining their own functioning. It is essential that the user is fully convinced that the mechanism's decision was correct. By incorporating receptive fields, the proposed authorial mechanism becomes capable of explaining its diagnoses in a creative and intelligent manner. Instead of relying on symmetric feature extractors, the authorial mechanism creates receptive fields from elements derived directly from the raw thermogram.

There are notable limitations in current anatomical disease detection mechanisms when evaluated against Alan Turing's postulates. Typically, diagnoses provided by computational tools are presented as labels without further explanation. In considering

thermographic images, the goal is to establish descriptions and patterns similar to those developed by the American College of Radiology [9].

The motivation is that lesions identified in thermography currently lack a self-descriptive technical standard. Artificial intelligence (AI) presents itself as a viable alternative. During its learning phase, AI is capable of analyzing thousands of files and extracting features from them. After learning, AI could establish patterns related to the shape, density, and neighboring region of the lesion. In this way, AI would gain the means to explain its decisions to a human.

**Figure 14**

*An authorial receptive field*

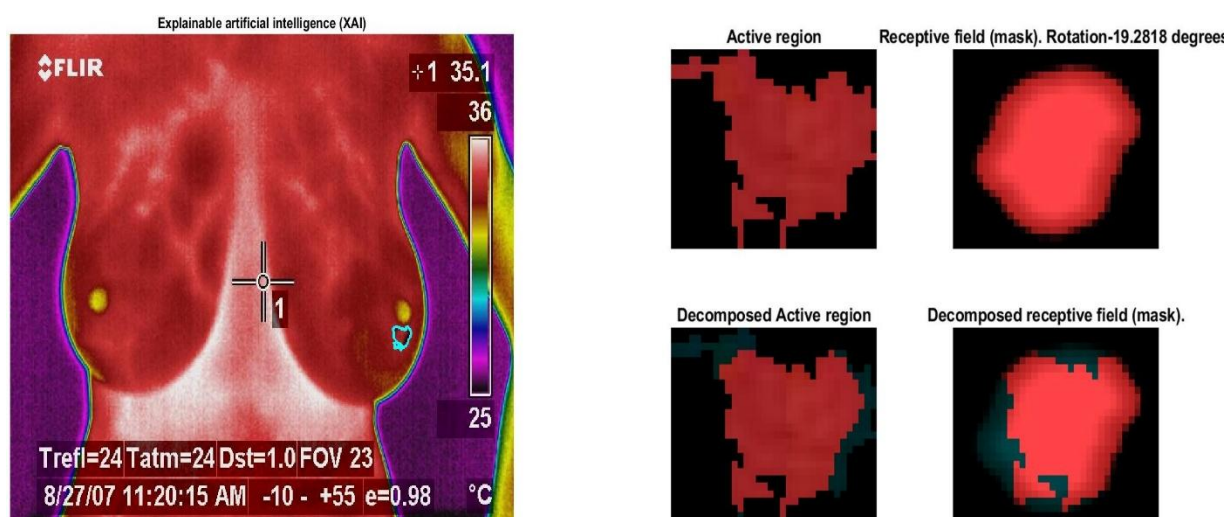


**Figure 15**

*QR code for video showing how authorial AI works*



The motivation is that lesions identified in thermography currently lack a self-descriptive technical standard. Artificial intelligence (AI) presents itself as a viable alternative. During its learning phase, AI is capable of analyzing thousands of files and extracting features from them. After learning, AI could establish patterns related to the shape, density, and neighboring region of the lesion. In this way, AI would gain the means to explain its decisions to a human.

A key operational challenge in traditional neural networks lies in their dependency on initial randomness. Synaptic connections between the weights  $w_{ji}$  of neurons in the input and hidden layers start randomly. In backpropagation-based networks, these synaptic connections gradually adjust to the target application by reducing the distance between desired and obtained responses.

If the random seed is suitable for a given application, the neural network will achieve excellent results. However, if the seed is unsuitable, the neural network may produce disastrous outcomes. Achieving satisfactory results in one application with a given initial random number seed does not guarantee that the same seed will yield good results in another application. Finding the optimal seed for generating random numbers can be a time-consuming problem, making exhaustive search computationally unfeasible.

A commonly employed alternative involves multiple executions of the same neural network architecture. Each execution uses a different initial random number seed. This approach allows for the assessment of whether variations in initial synaptic weights can significantly influence the results. At the end of the experiments, a high standard deviation would indicate that the results are dispersed, suggesting that the neural network is influenced by and dependent on the initial random conditions. In such cases, the initial conditions could abruptly either degrade or enhance the neural network's accuracy, making it risky to adopt such a solution in clinical practice, for example.

In the authorial self-explainable AI, synaptic connections are not determined randomly. Instead, they correspond to the receptive fields. The neural network's architecture itself provides resources to make the model self-explainable. The structure of the network, by directly reflecting in the receptive fields, plays a crucial role in the model's ability to provide clear and comprehensible explanations, promoting transparency and interpretability in the decision-making process.

Additionally, it is important to emphasize the comprehensibility of each of the nine neurons present in the authorial neural network architecture. These elements not only play a

fundamental role in executing the proposed technique but also serve as essential building blocks for explaining the system's operation. The transparency provided by the comprehensibility of the neurons in the single hidden layer significantly contributes to the user's confidence in the methodology.

This emphasis on comprehensibility not only enhances the effectiveness of the technique but also addresses the growing need for explainable systems in the field of artificial intelligence. This strategic focus strengthens the credibility of the proposal and highlights its potential impact on future clinical applications and advances in breast cancer prevention and detection.

All the data for this study is available at this GitHub link: <https://github.com/Gabriel09BR/XAI-Thermography>. Researchers can also access our statistical learning repository. This helps reproduce our experiment and verify the results without our influence. The repository also shows image decompositions at various levels to extract features from thermographic images. This addition of the feature extraction step increases the transparency and reliability of the proposed method.

### 3 RESULTS

This section presents the results of the proposed self-explainable artificial intelligence technique. Tens of thousands of receptive fields were generated for cysts, malignant lesions, and benign lesions, respectively. The high volume of receptive fields rendered the experiment computationally impractical within a reasonable timeframe. Investigating this volume of receptive fields across the entire database could take months, if not years.

To reduce dimensionality, this work selected statistically distinct receptive fields. Classical texture and shape descriptors, including Haralick moments, were employed to describe the receptive fields. The attributes derived from classical descriptions were subjected to both parametric and non-parametric statistical hypothesis tests. Only statistically distinct receptive fields were retained at the end of the experiment.

After the dimensionality reduction process, there were still hundreds of receptive fields (masks) for each target class cysts, malignant lesions, and benign lesions. This strategy optimized computational efficiency, but further dimensionality reduction was still necessary.

To optimize training time, the database was strategically divided into 20 batches, each containing randomly selected samples from all classes, including normal mammograms without apparent lesions. Using the one-against-all method, the accuracy of the receptive

fields was examined concerning the target class in each batch. At the end of each batch's evaluation, only the receptive fields with accuracy above the mean plus the standard deviation were retained for subsequent analysis.

In all scenarios and classes, investigating just three batches was sufficient to conclude the experiment and identify the selected receptive fields. During this phase of dimensionality reduction, it is important to note that there were only two neurons in the hidden layer, as described in

Eq. (7) and Eq. (8), without the support of the other neurons. This approach not only expedited response time but also highlighted that the selection of receptive fields was based exclusively on local information, without the influence of global information from the thermogram's color spectrum. This strategy reinforces the efficiency and independence of the dimensionality reduction process adopted.

Figures 16, 17, and 18 display the authorial descriptions following the work conducted by the American College of Radiology in the ACR BI-RADS®. The authorial AI bases its decisions in a manner comprehensible to humans. Additionally, this approach provides resources that enable specialists to justify their decisions to regulatory bodies, such as professional councils.

**Figure 16**

*Degree of accuracy for cysts*



**Figure 17**

*Degree of accuracy regarding benign lesions*

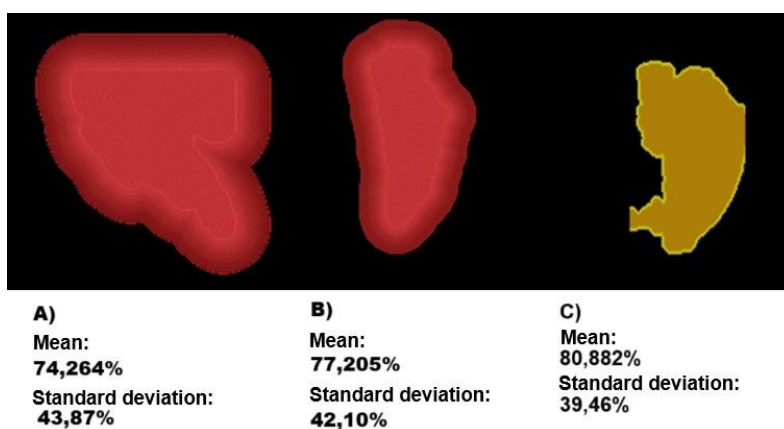


**Figure 18**

*Degree of accuracy regarding malignant lesions*

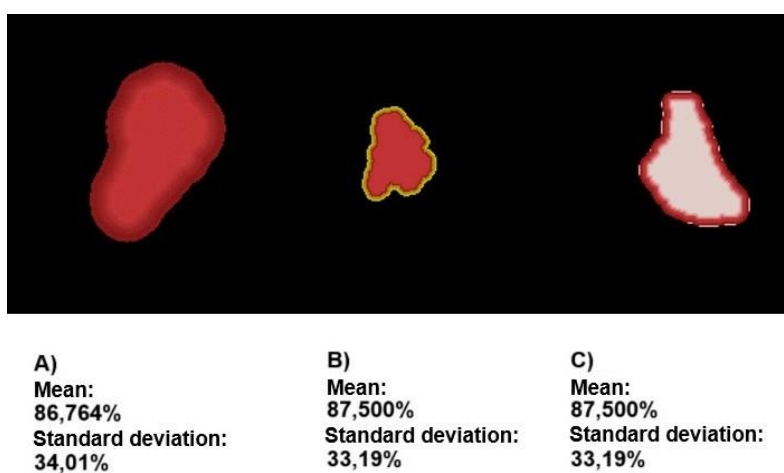


**Table 2**

*The accuracy of receptive fields as a function of class*

Class	Order of receptive fields	Accuracy (%)
Cist	1	84,55 % $\pm$ 36,26 %
	2	87,50 % $\pm$ 33,19 %
	3	88,23 % $\pm$ 32,33%
Benign lesion	1	74,26 % $\pm$ 43,87 %
	2	81,61 % $\pm$ 38,87 %
	3	82,35 % $\pm$ 38,26 %
Malignant lesion	1	87,50 % $\pm$ 33,19 %
	2	88,70 % $\pm$ 32,33 %
	3	89,70 % $\pm$ 30,50 %

The content of Table 1 pertains to the accuracy of the receptive fields described in Figure 16, Figure 17, and Figure 18. The accuracy and standard deviation results for the second and third masks of malignant lesions were found to be identical. Utilizing the one-vs-all method, the accuracy of the receptive fields was assessed relative to the target class across the entire dataset. The counter-class included all other classes, including cases of thermograms without lesions.

Each receptive field was subjected to individual experiments where the hidden layer, consisting of the self-explanatory neurons presented in Section 3.4, was employed in each pattern recognition task. Analysis of Table 1 reveals that the accuracy of the receptive fields is a critical metric for evaluating their impact on the system's decision-making process. The individual disposition and performance of each receptive field provide valuable insights into the specific contribution of each to the overall effectiveness of the model. This detailed approach enables a deeper understanding of the nuances in the pattern recognition process and highlights the relevance of self-explanatory neurons within the hidden layer.

Table 2 presents the confusion matrices of the receptive fields (masks) shown in Table 1, expressed in percentage terms. The confusion matrix is crucial for assessing the quality of supervised learning. In Table 2, "C." and "CC." are abbreviations for Class and Counter-Class, given that the training method is one-vs-all. The desired classes are listed on the

vertical label, while the counter-classes are on the horizontal label. In the confusion matrix, the main diagonal is occupied by instances where the predicted class matches the expected class, referred to as true positive cases. Thus, a good classifier is characterized by a high concentration of values along the main diagonal, with lower values in other elements.

Table 2 highlights the main diagonals in bold. Concerning cyst classification, the first receptive field incorrectly classified, on average, 4.76% of cases as cysts when they belonged to other classes (benign lesions, malignant lesions, and patients without lesions). Similarly, an average of 51.61% of counter-class cases were classified as cysts when they involved patients with cysts.

Moreover, Table 2 indicates that sensitivity and specificity refer to the capacity of the receptive field (mask) to recognize samples from the class and counter-class, respectively. The proposed work presents the confusion matrix in percentage terms to facilitate the interpretation of sensitivity and specificity. In summary, sensitivity and specificity are presented within the confusion matrix described in Table 2. For instance, the first receptive field associated with cysts shows an average sensitivity of 48.39% regarding true positives. Similarly, this same mask achieves an average specificity of 95.24% concerning true negatives.

Presenting the confusion matrix in percentage terms is important because it allows for the inference of many metrics related to statistical classification. For example, metrics such as prevalence, precision,

MCC, FM, ROC curve, and AUC curve, are derived from the confusion matrix. Dozens of metrics can be extracted from the confusion matrix presented in Table 2.

### 3.1 PATTERN RECOGNITION WITH OPTIMIZED WEIGHTS

Accuracy refers to the classifier's ability to detect samples from both the class and the counter-class. It differs from precision, which does not favor the counter-class. For instance, precision plays a fundamental role in the field of biomedical engineering. The objective is to detect all patients with abnormalities in the breast parenchyma (e.g., breast cancer), even if this means that some healthy patients might be erroneously diagnosed as ill. The advantages are substantial, considering that early detection of cancer through imaging is crucial for increasing a patient's chances of recovery [44].

For each detection of a patient with cancer in an imaging examination, thousands of tests are needed for healthy patients. In this context, prioritizing precision over accuracy is

essential to ensure that cancer patients are not missed. This is particularly valid in developing and emerging countries, where a large portion of the population has difficulty accessing public health services such as hospitals and diagnostic clinics [46].

Additionally, there is a significant income disparity [47], where a substantial segment of society cannot afford care in private clinics and hospitals. Moreover, most of the population lives in pockets of poverty located on the outskirts of major urban centers in emerging countries [48], and a large part of the population does not have a fixed residence [49], [50]. Consequently, scheduling follow-up consultations or tests becomes impractical. Poor income distribution, poverty pockets, and the overload of public health services are recurring issues in developing nations [51], [52].

In emerging countries, a thermographic imaging examination may be a unique opportunity for a patient. Moreover, a significant portion of the care provided in public health services occurs at the terminal stages of diseases [53]. A significant proportion of deaths reported with poorly defined causes might be due to insufficient time for investigating and certifying the causes of death [53].

In summary, emphasizing precision over accuracy is crucial in biomedical applications when used in emerging countries. In such scenarios, failing to detect a patient with cancer cannot be afforded, even if it results in false positives or healthy patients being wrongly classified as ill. In biomedical engineering, the disadvantage of increasing precision at the expense of accuracy is acceptable. The patient may suffer temporary psychological trauma until a biopsy is performed to confirm or refute the preliminary diagnosis. It is recommended that a positive diagnosis through imaging not be disclosed to the patient, as it is an immature result pending confirmation.

The current explainable artificial intelligence investigates the best way to determine the  $n$ -dimensional space to achieve a high precision rate concerning the target class. Here,  $n$  refers to the number of input neurons. This section aims to increase precision for classes with unbalanced samples.

The proposed work extends the study of [54] and creates a weight matrix named "percentage," formalized in Eq. (10). Here,  $v$  refers to the training data. When considering  $P_{tt}$  as a two-dimensional matrix, the positions  $tt$  denote the diagonal matrix, where  $t = 1, \dots, v$ . The symbol  $:=$  indicates the number of cases per class.  $\zeta$  represents the number of classes (e.g., class versus counter-class).

$$P_{tt} = 1/(X\zeta) \quad (10)$$

By assigning weighted measures to the classes, the output weight matrix  $\beta$  is in accordance with Eq. (11). Here,  $I$  is the identity matrix, and  $P$  is the weighted matrix based on the classes with imbalanced quantities, as described in Eq. (10). The superscript  $T$  denotes the transpose of a matrix.

$$\beta = H \cdot ((P \cdot H^T \cdot H + I_w) / ((P \cdot T^T) \cdot H)) \quad (11)$$

**Table 3**

*The accuracy of receptive fields according to class, with optimized weights*

Class	Order of receptive fields	Accuracy (%)
Cist	1	68,38 % ± 46,67 %
	2	67,64 % ± 46,95 %
	3	64,70 % ± 47,96 %
Benign lesion	1	64,70 % ± 47,96 %
	2	66,91 % ± 47,22 %
	3	66,91 % ± 47,22 %
Malignant lesion	1	72,05 % ± 45,03 %
	2	70,58 % ± 45,73 %
	3	77,94 % ± 41,61 %

**Table 4**

*Confusion matrix of receptive fields according to class, with optimized weights*

Class	Order of receptive fields		C	CC
Cist	1	C	<b>77,42 %</b>	34,29 %
		CC	22,58 %	<b>65,71 %</b>
	2	C	<b>83,87 %</b>	37,14 %
		CC	16,13 %	<b>62,86 %</b>
	3	C	<b>87,10 %</b>	41,90 %
		CC		

		CC	12,90 %	<b>58,10 %</b>
	1	C	<b>69,39 %</b>	37,93 %
		CC	30,61 %	<b>62,07 %</b>
Benign lesion	2	C	<b>69,39 %</b>	34,48 %
		CC	30,61 %	<b>65,52 %</b>
	3	C	<b>73,47 %</b>	36,78 %
		CC	26,53 %	<b>63,22 %</b>
	1	C	<b>72,73 %</b>	28,16 %
		CC	27,27 %	<b>71,84 %</b>
Malignant lesion	2	C	<b>72,73 %</b>	30,10 %
		CC	27,27 %	<b>69,90 %</b>
	3	C	<b>84,85 %</b>	24,27 %
		CC	15,15 %	<b>75,73 %</b>

Table 3 pertains to the accuracy of the receptive fields described in Figure 16, Figure 17, and Figure 18. Using the one-against-all method, the accuracy of the receptive fields was examined in relation to the target class across the entire dataset. In the counter-class, all other classes were included, including cases of thermograms without lesions. Each receptive field was subjected to individual experiments, where the hidden layer, composed of self-explanatory neurons presented in Section 3.4, was used in each pattern recognition task.

Table 3 presents the receptive fields (masks) in percentage terms. Table 4 shows the confusion matrices of the receptive fields (masks), with the main diagonals emphasized in bold. Regarding the Cyst, the first receptive field incorrectly classified, on average, 34.29% of cases as cysts when they were actually cases of other classes (benign lesion, malignant lesion, and patients without lesions). Similarly, there was an average misclassification rate of 22.58% of counter-class cases when they were, in fact, patients with cysts (false negatives).

It is observed that the purpose of the weighted measures is not to increase the overall accuracy of the solution, but rather to improve precision, aiming to reduce the number of false negatives. When comparing the original approach, as shown in Table 2, with the current approach incorporating weighted measures, it is evident that false negatives have been significantly reduced from 51.61% to 22.58% for the first cyst receptive field. In the most optimized scenario, only 12.90% of patients affected by cysts were not identified by the

current self-explanatory artificial intelligence, using the third receptive field developed for cysts.

#### **4 DISCUSSION**

The self-explanatory artificial intelligence developed here was able to achieve accuracy levels comparable to state-of-the-art Deep Learning models. Additionally, the accuracy provided by this AI offers both confidence and interpretability in the results. The proposed AI not only achieves high accuracy but also transparently explains the reasoning behind its decisions, making it particularly valuable in settings where understanding model behavior is crucial.

A self-explanatory AI also aids in identifying potential biases or systematic errors within the model, which is essential for preventing discriminatory decisions or reliance on undesirable patterns. Its explainability increases acceptance and trust among users and professionals, who may otherwise resist adopting machine learning models due to their opaque decision-making processes. By providing insights into causal relationships within the data, self-explanatory models allow users to understand which variables most influence the model's outcomes.

In regulated sectors, the ability to explain decisions can be a legal requirement, and self-explanatory models facilitate compliance with both regulations and ethical standards. This interpretability also fosters better collaboration between humans and machines, especially in complex tasks where human expertise is essential.

Despite these advantages, self-explanatory AI faces challenges in scalability and generalization. Its effectiveness relies on well-categorized data, which can limit performance in settings with limited or diverse data, making it harder to generalize across different scenarios and patient profiles. Implementing such models on a large scale may also prove challenging, especially in clinical environments with limited computational resources, as generating detailed explanations can be computationally demanding. Additionally, although this model supports bias identification, it may inadvertently reinforce discriminatory patterns if biases are present in the training data, necessitating rigorous audits to ensure that explanations remain free from biased interpretations. In summary, the combination of high accuracy and explainability enhances the practical utility, reliability, and acceptance of AI across various contexts, promoting a more effective and ethical integration of artificial intelligence into society.

This research presents significant contributions to the field of biomedical engineering and breast cancer detection, especially in the context of medical imaging and artificial intelligence. The key contributions are:

**Development of a Self-Explainable AI-Based Diagnostic Tool:** we propose an intelligent system for detecting and classifying breast lesions in thermographic images. We use extreme learning machines (ELM) for this purpose. The proposed approach is self-explanatory. This means that healthcare professionals can easily understand and validate the reasoning behind each automated diagnosis. This is different from traditional black-box deep learning models. In a clinical environment, this is very important. Accountability and transparency are important for patient care and professional validation.

**Integration of Low-Complexity AI Techniques with Biomedical Imaging:** deep learning methods show excellent results, but are costly from a computational time point of view. They are also difficult to interpret. This work uses extreme learning neural networks. This AI model has low computational complexity without degrading the results. Extreme learning offers a fast, efficient and affordable option for breast cancer screening. It works well in low-resource environments, making it more accessible to everyone.

**Creating a technical standard for the analysis of thermographic lesions:** this research aims to standardize the classification of breast lesions in thermographic images. It is inspired by the BI-RADS system used in mammography. The author's standardization does this by looking at the shapes, texture and area occupied by breast lesions. This initiative fills a gap in clinical practice. It provides a useful reference for professionals using thermographic breast cancer detection.

**Improved early detection and patient outcomes:** our approach finds malignant lesions faster and more accurately. This leads to a better prognosis with timely intervention. It helps with breast conservation therapy by improving early diagnosis. This reduces the need for major surgery, such as mastectomy.

## **5 CONCLUSION**

The primary goal of this study was to improve recovery prospects for patients diagnosed with breast cancer, aiming to significantly reduce its prevalence as a leading cause of mortality among the Brazilian population. In the specific context of breast cancer, the project seeks to contribute to early diagnosis and minimize the need for radical surgeries, such as mastectomy, when they are not strictly necessary. It is hoped that the developed

system will be integrated into the hospital network, playing a crucial role in the identification and interpretation of breast lesions. The desired impact is that the efficiency and accuracy of breast examinations become less dependent on the subjective interpretation and individual experience of the examining professional. Furthermore, it is expected that the results of this research will be considered in future updates to the Ministry of Health's consensus document on breast cancer.

Image-based diagnosis is challenging due to the variability of cases and the sheer volume of data. To enhance diagnosis, image processing techniques are applied to identify objects with computational precision. However, the search for optimal configurations for these techniques is complex and requires supercomputers due to the vast exploration space. Although deep neural networks (Deep Learning) are used in state-of-the-art methods to recognize patterns in medical images, they have disadvantages such as long training times and the difficulty in explaining their decisions due to their millions of trainable parameters. These limitations can be overcome using extreme learning techniques, which are computationally efficient and more interpretable. This project proposes to employ extreme learning in the detection and classification of lesions in thermographic images. The goal is to develop an application capable of intelligently and convincingly explaining its functioning and diagnoses to medical specialists.

The emphasis on explainable artificial intelligence is fundamental, as it ensures that academic advances are not restricted. If a computational tool, even if accurate, has limitations in explaining its own functioning, it may be discarded in favor of more traditional methods. This commitment to system transparency and comprehensibility reflects the pursuit of technological solutions that are not only effective but also accessible and understandable. This project argues that the mere correct functionality of a computational technique is not sufficient; it is essential that the mechanisms have the ability to explain their decision-making processes, thereby providing the user with full confidence in the system's decisions.

In a systematic manner, the proprietary intelligent technique will be submitted to high-impact journals and conferences. Additionally, the project will seek patent registration for both the general workflow of the project and for potential proprietary features extracted from biomedical images. The expectation is that the state of Pernambuco will assume a prominent position in the prevention and automated detection of breast cancers, providing an explainable and reliable approach.

## 5.1 CHALLENGES ENCOUNTERED

During the research, several obstacles were encountered, such as the low resolution of some images in the database. Not all images were captured with the same resolution; therefore, these images were removed during preprocessing to avoid compromising the model's efficiency and accuracy.

Another challenge was the possibility of developing a 3D model, given that there were images captured from different angles. Additionally, the images were disorganized, and not all necessary positions were obtained for some patients. To avoid a drastic reduction in the dataset, this approach was not pursued.

These obstacles highlight the importance of having a high-quality and well-organized database to improve machine learning model outcomes. Future research may focus on standardizing collected images and organizing the data to facilitate the development of more complex and accurate models. Moreover, interpolation and image reconstruction techniques could be explored to handle low-resolution or missing images, enabling the creation of more complete and detailed 3D models.

## 5.2 FUTURE WORK

During the development of this research, two aspects emerged that merit further investigation.

(i) The idea of enhancing the image preprocessing to make it more efficient. By optimizing the methods involved in preprocessing, it is anticipated that not only the processing time will be significantly reduced, but also the quality of the resulting images will be improved. This may include advanced techniques such as filtering, noise reduction, intensity normalization, and edge enhancement. Enhancing these techniques could lead to a more accurate and faster analysis of subsequent images. By achieving greater precision and accuracy in preprocessing, machine learning and pattern recognition models can operate more effectively, resulting in more reliable diagnoses and better-informed decisions.

(ii) Another potential research direction would be the development of affective computing to help machines explain their diagnoses to specialists. Affective computing could make interactions more intuitive and empathetic, facilitating the understanding of information provided by the machine. With this technology, the machine could offer detailed and technical explanations for experienced specialists, while presenting information in a more simplified and accessible manner for professionals less familiar with the system. This level of

customization would not only improve the usability of the program but also increase the specialists' confidence in automated decisions, promoting a more effective integration of artificial intelligence in the clinical environment.

### 5.3 COMPLIANCE WITH ETHICAL STANDARDS

**Conflict of interest:** The authors declare that they have no conflict of interest.

**Research Involving Human Participants and/or Animals:** The authors declare that no human participants were involved in this research.

**Informed Consent:** This research did not include healthcare intervention of human participants.

**Funding:** This research received no external funding.

**Data Availability Statement:** All data supporting the findings of this study are openly available at the following GitHub repository: <https://github.com/Gabriel09BR/XAI-Thermography> .

## ACKNOWLEDGMENTS

We would like to thank the University of Pernambuco (UPE) for providing the opportunity to develop this research and for the support offered throughout the project.

**Author contributions:** Gabriel Luiz Limeira Barreto and Professor Sidney Marlon Lopes de Lima jointly conceived and developed the methodology proposed in this study. Both authors contributed to the design of the self-explainable artificial intelligence model and the definition of the computational architecture. Gabriel Luiz Limeira Barreto was primarily responsible for the implementation, preprocessing of thermographic images, and execution of the experiments. Professor Sidney Marlon Lopes de Lima provided theoretical support, guided the experimental design, and critically reviewed the manuscript to ensure its scientific consistency.

## REFERENCES

- [1] "Dados e Números sobre Câncer de Mama - Relatório Anual 2023." 2023. Accessed: Apr. 09, 2025. [Online]. Available: <https://www.inca.gov.br/publicacoes/relatorios/dados-e-numeros-sobre-cancer-de-mama-relatorio-anual-2023>

- [2] "INCA: Controle do Câncer de Mama - Documento de Consenso," Rev Brasil Cancerologia, v. 50, n. 2, p. 77-90, 2004, doi: DOI: 10.32635/2176-9745.RBC.2004v50n2.2039.
- [3] "Global Cancer Observatory. World Health Organization. Globocan, 2022." 2022. Accessed: Apr. 09, 2025. [Online]. Available: <https://gco.iarc.who.int/today/en/fact-sheets-populations#regions>
- [4] "INCA: Instituto Nacional do Câncer; Orientações fisioterápicas: mastologia." 2011.
- [5] J. H. Juhl, A. B. Crummy, and J. E. Kuhlman, Interpretação Radiológica., 7th ed. Guanabara, 2014.
- [6] W. Leucht and D. Leucht, Teaching Atlas of Breast Ultrasound., 2nd ed. Georg Thieme Verlag, Thieme Medical Publishers, 1996.
- [7] K. J. W. Taylor et al., "Ultrasound as a complement to mammography and breast examination to characterize breast masses," Ultrasound Med Biol, vol. 28, no. 1, pp. 19–26, Jan. 2002.
- [8] S. Gefen et al., ROC analysis of ultrasound tissue characterization classifiers for breast cancer diagnosis, vol. 22. 2003. doi: 10.1109/TMI.2002.808361.
- [9] et al. D'Orsi CJ Sickles EA, Mendelson EB, Morris EA, ACR BI-RADS® Atlas, Breast Imaging Reporting and Data System. Reston, VA. American College of Radiology. 2013. Accessed: Apr. 09, 2025. [Online]. Available: <https://www.acr.org/Clinical-Resources/Reporting-and-Data-Systems/Bi-Rads>
- [10] M. D. Heath and K. W. Bowyer, "Mass Detection by Relative Image Intensity.," 5th International Conference on Digital Mammography. Toronto, Canada, June. Medical Physics Publishing (Madison, WI), ISBN 1-930524-00-5, 2000.
- [11] S. M. L. Lima, A. G. Silva-Filho, and W. P. Dos Santos, A methodology for classification of lesions in mammographies using Zernike Moments, ELM and SVM Neural Networks in a multi-kernel approach. doi: <https://doi.org/10.1109/SMC.2014.6974041>, 2014.
- [12] W. W. Azevedo et al., Fuzzy Morphological Extreme Learning Machines to detect and classify masses in mammograms. 2015. doi: 10.1109/FUZZ-IEEE.2015.7337975.
- [13] W. W. Azevedo et al., Morphological extreme learning machines applied to detect and classify masses in mammograms. 2015. doi: 10.1109/IJCNN.2015.7280774.
- [14] W. W. A. da Silva, M. A. de Santana, A. G. da S. Filho, S. M. L. de Lima, and W. P. dos Santos, Chapter 3 - Morphological extreme learning machines applied to the detection and classification of mammary lesions. in Hybrid Computational Intelligence for Pattern Analysis and Understanding. Academic Press, 2021. doi: 10.1016/B978-0-12-819295-5.00003-2.

- [15] S. M. L. de Lima, A. G. da Silva-Filho, and W. P. dos Santos, Detection and classification of masses in mammographic images in a multi-kernel approach, vol. 134. 2016. doi: 10.1016/j.cmpb.2016.04.029.
- [16] J. M. S. et al. Pereira, Method for Classification of Breast Lesions in Thermographic Images Using ELM Classifiers. In: SANTOS, W.P.; SANTANA, M.A.; SILVA, W.W.A. Understanding a Cancer Diagnosis. Disponível em: <https://novapublishers.com/shop/understanding-a-cancer-diagnosis/>, 2020.
- [17] J. M. S. Pereira et al., “Feature selection based on dialectics to support breast cancer diagnosis using thermographic images.,” Res. Biomed. Eng. 37, pp. 485–506, 2021.
- [18] M. C. Araújo, R. C. F. Lima, and R. M. C. R. de Souza, “Interval symbolic feature extraction for thermography breast cancer detection,” Expert Systems with Applications, vol. 41, no. 15, pp. 6728–6737, 2014, doi: <https://doi.org/10.1016/j.eswa.2014.04.027>.
- [19] T. B. Borchardt, A. Conci, R. C. F. Lima, R. Resmini, and A. Sanchez, “-,” Signal Processing, vol. 93, no. 10, pp. 2785–2803, 2013, doi: <https://doi.org/10.1016/j.sigpro.2012.08.012>.
- [20] S. Ekici and H. Jawzal, “Breast cancer diagnosis using thermography and convolutional neural networks,” Medical Hypotheses, vol. 137, p. 109542, 2020, doi: <https://doi.org/10.1016/j.mehy.2019.109542>.
- [21] C. N. Karim, O. Mohamed, and T. Ryad, “A new approach for breast abnormality detection based on thermography,” Medical Technologies Journal, 2018, Accessed: Apr. 09, 2025. [Online]. Available: <https://api.semanticscholar.org/CorpusID:69778691>
- [22] A. Morales-Cervantes et al., “An automated method for the evaluation of breast cancer using infrared thermography,” EXCLI J, vol. 17, pp. 989–998, Oct. 2018.
- [23] A. M. Turing, “Computing Machinery and Intelligence, Mind.,” Issue 236, October 1950, Pages 433–460, vol. LIX, 1950, doi: <https://doi.org/10.1093/mind/LIX.236.433>.
- [24] M. Macedo, M. Santana, W. P. dos Santos, R. Menezes, and C. Bastos-Filho, “Breast cancer diagnosis using thermal image analysis: A data-driven approach based on swarm intelligence and supervised learning for optimized feature selection,” Applied Soft Computing, vol. 109, Sep. 2021, Accessed: Apr. 09, 2025. [Online]. Available: <https://www.sciencedirect.com/science/article/pii/S1568494621004567>
- [25] de F. Barbosa and de C. F. de Lima, “Combining deep-wavelet neural networks and support-vector machines to classify breast lesions in thermography images.,” Health Technol. 12, 2022, doi: <https://doi.org/10.1007/s12553-022-00705-3>.
- [26] dos Santos, “A deep-wavelet neural network to detect and classify lesions in mammographic images.,” Res. Biomed. Eng. 38, 2022, doi: <https://doi.org/10.1007/s42600-022-00238-8>.

- [27] S. M. L. Lima and W. P. Santos, Morphological Decomposition to Detect and Classify Lesions in Mammograms. In: Wellington Pinheiro dos Santos; Maíra Araújo de Santana; Washington Wagner Azevedo da Silva. (Org.). Understanding a Cancer Diagnosis. Disponível em: <https://novapublishers.com/shop/understanding-a-cancer-diagnosis/>, 2020.
- [28] K. Niu and C. Tian, "Zernike polynomials and their applications," Journal of Optics, vol. 24, no. 12, p. 123001, Nov. 2022, doi: 10.1088/2040-8986/ac9e08.
- [29] A. Tahmasbi, F. Saki, and S. B. Shokouhi, "Classification of benign and malignant masses based on Zernike moments," Computers in Biology and Medicine, vol. 41, no. 8, pp. 726–735, 2011, doi: <https://doi.org/10.1016/j.compbimed.2011.06.009>.
- [30] D. Papalia, S. Olds, and R. Feldman, Human Development. The McGraw-Hill Companies, 11a edição, pág. 162, 2008.
- [31] S. Shalev-Shwartz and J. Shai Ben-David, Understanding Machine Learning: From Theory To Algorithms. Cambridge University Press., 2014.
- [32] J. Ba and R. Caruana, "Do Deep Nets Really Need to be Deep?," in Advances in Neural Information Processing Systems, Z. Ghahramani, M. Welling, C. Cortes, N. Lawrence, and K. Q. Weinberger, Eds., Curran Associates, Inc., 2014. Accessed: Apr. 09, 2025. [Online]. Available: [https://proceedings.neurips.cc/paper\\_files/paper/2014/file/ea8fcd92d59581717e06eb187f10666d-Paper.pdf](https://proceedings.neurips.cc/paper_files/paper/2014/file/ea8fcd92d59581717e06eb187f10666d-Paper.pdf)
- [33] S. M. L. Lima et al., "Next-generation antivirus endowed with web-server Sandbox applied to audit fileless attack," Soft Computing, vol. 27, no. 3, pp. 1471–1491, Feb. 2023, doi: 10.1007/s00500-022-07447-4.
- [34] M. M. Mijwil, "Smart architectures: computerized classification of brain tumors from MRI images utilizing deep learning approaches," Multimed Tools Appl, vol. 84, no. 5, pp. 2261–2292, Feb. 2025, doi: 10.1007/s11042-024-20349-x.
- [35] F. Chollet, "Xception: Deep Learning with Depthwise Separable Convolutions," 2017 IEEE Conference on Computer Vision and Pattern Recognition (CVPR), 2017, doi: 10.1109/CVPR.2017.195.
- [36] J. L. Patterson D. A. ., Hennessy, Computer Organization and Design., 5th ed. Morgan Kaufmann, 2013.
- [37] R. P. Pinheiro et al., "Antivirus applied to JAR malware detection based on runtime behaviors," Scientific Reports, vol. 12, no. 1, p. 1945, Feb. 2022, doi: 10.1038/s41598-022-05921-5.
- [38] M. M. dos Santos, A. G. da S. Filho, and W. P. dos Santos, Deep convolutional extreme learning machines: Filters combination and error model validation, vol. 329. 2019. doi: 10.1016/j.neucom.2018.10.063.

- [39] C. Xiang, S. Q. Ding, and T. H. Lee, "Geometrical interpretation and architecture selection of MLP," *IEEE Transactions on Neural Networks*, vol. 16, no. 1, pp. 84–96, 2005, doi: 10.1109/TNN.2004.836197.
- [40] G.-B. Huang, Y.-Q. Chen, and H. A. Babri, "Classification ability of single hidden layer feedforward neural networks," *IEEE Transactions on Neural Networks*, vol. 11, no. 3, pp. 799–801, 2000, doi: 10.1109/72.846750.
- [41] G.-B. Huang, H. Zhou, X. Ding, and R. Zhang, "Extreme Learning Machine for Regression and Multiclass Classification," *IEEE Transactions on Systems, Man, and Cybernetics, Part B (Cybernetics)*, vol. 42, no. 2, pp. 513–529, 2012, doi: 10.1109/TSMCB.2011.2168604.
- [42] M. A. de Santana et al., "Breast cancer diagnosis based on mammary thermography and extreme learning machines," *Research on Biomedical Engineering*, vol. 34, no. 1, pp. 45–53, Jan. 2018, doi: 10.1590/2446-4740.05217.
- [43] M. Z. do Nascimento, A. S. Martins, L. A. Neves, R. P. Ramos, E. L. Flores, and G. A. Carrijo, "Classification of masses in mammographic image using wavelet domain features and polynomial classifier," *Expert Systems with Applications*, vol. 40, no. 15, pp. 6213–6221, 2013, doi: <https://doi.org/10.1016/j.eswa.2013.04.036>.
- [44] S. M. L. de Lima et al., "Artificial intelligence-based antivirus in order to detect malware preventively," vol. 10. 2021. doi: 10.1007/s13748-020-00220-4.
- [45] "XAI-Thermography." 2023. Accessed: Apr. 10, 2025. [Online]. Available: <https://github.com/Gabriel09BR/XAI-Thermography>
- [46] M. Kremer and R. Glennerster, "Chapter Four - Improving Health in Developing Countries: Evidence from Randomized Evaluations.," in *Handbook of Health Economics*, vol. 2, M. V. Pauly, T. G. McGuire, and P. P. Barros, Eds., in *Handbook of Health Economics*, vol. 2. , Elsevier, 2011, pp. 201–315. doi: 10.1016/B978-0-444-53592-4.00004-9.
- [47] F. Alvaredo and L. Gasparini, "Chapter 9 - Recent Trends in Inequality and Poverty in Developing Countries," in *Handbook of Income Distribution*, vol. 2, A. B. Atkinson and F. Bourguignon, Eds., in *Handbook of Income Distribution*, vol. 2. , Elsevier, 2015, pp. 697–805. doi: 10.1016/B978-0-444-59428-0.00010-2.
- [48] "Instituto Brasileiro de Geografia e Estatística: Domicílios particulares ocupados em aglomerados subnormais e Média de moradores em domicílios particulares ocupados em aglomerados subnormais." 2023. Accessed: Apr. 09, 2025. [Online]. Available: <https://sidra.ibge.gov.br/tabela/3380>
- [49] E. T. Paulino, "The agricultural, environmental and socio-political repercussions of Brazil's land governance system," *Land Use Policy*, vol. 36, pp. 134–144, 2014, doi: <https://doi.org/10.1016/j.landusepol.2013.07.009>.

- [50] B. P. Reydon, V. B. Fernandes, and T. S. Telles, "Land tenure in Brazil: The question of regulation and governance," *Land Use Policy*, vol. 42, pp. 509–516, 2015, doi: <https://doi.org/10.1016/j.landusepol.2014.09.007>.
- [51] "Organização Mundial da Saúde: Improving the quality and use of birth, death and cause-of-death information: guidance for a standards-based review of country practices," ISBN: 9789241547970, 2010.
- [52] "Food and Agriculture Organization of the United Nations - Organização das Nações Unidas para Alimentação e Agricultura) Developing Country Regions," \hspace{0.10cm}, 3AD.
- [53] E. B. França et al., "Investigation of ill-defined causes of death: assessment of a program's performance in a state from the Northeastern region of Brazil," *Rev Bras Epidemiol*, vol. 17, no. 1, pp. 119–134, Jan. 2014.
- [54] W. Zong, G.-B. Huang, and Y. Chen, "Weighted extreme learning machine for imbalance learning," *Neurocomputing*, vol. 101, pp. 229–242, 2013, doi: <https://doi.org/10.1016/j.neucom.2012.08.010>.